Surface-Dependent Activation of Model α-Al2O3-Supported P-Doped Hydrotreating Catalysts Prepared by Spin Coating

Ricardo Garcia de Castro, Jérémy Bertrand, Baptiste Rigaud, Elodie Devers, Mathieu Digne, Anne-félicie Lamic-Humblot, Gerhard Pirngruber, Xavier Carrier

Surface-dependent activation of model α-Al_2O_3-supported P-doped hydrotreating catalysts prepared by spin coating

Ricardo GARCIA DE CASTRO,[1,2] Jérémy BERTRAND,[1] Baptiste RIGAUD,[3] Elodie DEVERS,[2] Mathieu DIGNE,[2] Anne-Félicie LAMIC-HUMBLOT,[1] Gerhard D. PIRNGRUBER,[2] Xavier CARRIER[1,*]

1- Sorbonne Université, CNRS, Laboratoire de Réactivité de Surface, 75005 Paris (France)

2- IFP Energies nouvelles, Rond-point de l'échangeur de Solaize, 69360 Solaize (France)

3- Sorbonne Université, CNRS, Institut des Matériaux de Paris Centre, 75005 Paris (France)

*xavier.carrier@sorbonne-universite.fr

Abstract

Requirements for improved catalytic formulations is continuously driving research in sulfide-based catalysis for biomass upgrading and heteroatom removal for cleaner fuels. The present work proposes a surface-science approach for the understanding of the genesis of the active (sulfide) phase in model P-doped MoS_2 catalysts supported on α-Al_2O_3 single crystals. This approach allows one to obtain a surface-dependent insight by varying the crystal orientations of the support. Model phosphorus-doped catalysts are prepared via spin-coating of Mo-P precursor solutions onto four α-Al_2O_3 crystal orientations, C(0001), A($11\bar{2}0$), M($10\bar{1}0$) and R($1\bar{1}02$), that exhibit different natures of surface –OH. ^{31}P and ^{95}Mo liquid-state NMR are used to give a comprehensive description of the Mo and P speciations of the phospho-molybdic precursor solution. The speciation of the deposition solution is then correlated with the genesis of the active MoS_2 phase. XPS quantification of the surface P/Mo ratio reveal a surface-dependent phosphate aggregation driven by the amount of free phosphates in solution. Phosphates aggregation decreases in the following order C(0001) >> M($10\bar{1}0$) > A($11\bar{2}0$), R($1\bar{1}02$). This evolution can be rationalized by an increasing strength of phosphate/surface interactions on the different α-Al_2O_3 surface orientations from the C(0001) to the R($1\bar{1}02$) plane. Retardation of the sulfidation with temperature is observed for model catalysts with the highest phosphate dispersion on the surface (A($11\bar{2}0$), R($1\bar{1}02$)), suggesting that phosphorus strongly intervenes in the genesis of the active phase through a close intimacy between phosphates and molybdates. The apparent (XPS-based) surface P/Mo ratio appears as a key descriptor to quantify this retarding effect. It is proposed that retardation of sulfidation is driven by two effects: i) a chemical inhibition through formation of hardly reducible mixed molybdo-phosphate Al-O-Mo-P structures and ii) a physical inhibition with phosphate clusters inhibiting the growth of MoS_2. The sulfidation degree may thus be heterogeneous over the different facets of γ-Al_2O_3 particles. The surface-dependent phosphorus doping on model α-Al_2O_3 supports can be used as a guide for the rational design of more efficient HDT catalysts on industrial γ-Al_2O_3 carrier.

1. Introduction

In the current industrial context, the demand for more efficient heterogeneous catalysts drives the academic and industrial research towards a molecular-scale description of such materials. A very important part of this description is devoted to the understanding of the role of the support on the properties of the active phase upon different synthesis stages and on the overall catalytic activity. A remarkable example in which considerable effort has been invested in understanding of the support effect are hydrotreating catalysts. Hydrotreating is the industrial process designed for the removal of heteroatoms (mainly sulfur) under hydrogen atmosphere. The development of hydrotreating technology is a natural outcome from tightening environmental regulations, where a growing demand for cleaner fuels require more efficient hydrotreating catalysts. The current EU fuel specification for the sulfur content in oil fractions (*Euro V, 2009*) establishes a limit of 10 ppm of sulfur for diesel and gasolines[1] and Internal Marine Organization (IMO) a limit of 0.5 wt% for marine fuels since January 2020.[2] Hydrotreating catalysts are also key players for upgrading biofuels namely through the removal of oxygen (hydrodeoxygenation). The most active HDT catalysts are cobalt or nickel promoted MoS_2 or WS_2, typically supported on γ-Al_2O_3.[3],[4,5],[6] Nowadays, there is a general agreement regarding the nature of the active phase, the promotion sites[6–15], the additives that enhance the hydrodesulfurization (HDS) activity[16–21], and the structure of the porous support.[22,23] However, despite this rather complete description of HDT catalysts, the role that the support exerts on the genesis of the active phase is still poorly understood, while it is a major player in the molecular design of optimized catalysts. Properties such as slab length, stacking number and sulfidation degree of the sulfide active phase are influenced to a great extent by the nature and strength of the active phase-support interactions.[24–28] The influence of the support on the aforementioned properties have been studied from different perspectives. For instance, some research has been devoted to the surface chemistry of the support and its effect on the active phase[27,29] while others focused on the influence of the surface orientation[26,30] (planes (111) or (100) of γ-Al_2O_3, for instance). However, molecular-scale understanding of the role of the support cannot be thoroughly accomplished using traditional polycrystalline alumina powder supports (γ-Al_2O_3) since this transition alumina exposes different surfaces and a wide variety of surface –OH groups (sorption sites for the active precursors) which prevents a direct assessment of the individual reactivity of alumina surface facets. Synthesis efforts have been carried out in order to control the proportion of the different γ-Al_2O_3 facets, but even in favorable cases,[31] the (110) plane remains largely predominant and varying the proportion of the different γ-Al_2O_3 facets will remains difficult.

Planar (model) surfaces traditionally used in surface-science studies are interesting surrogates for powder supports in order to tackle the support effect since well-defined surfaces of varying surface structure can be used.[32] Some research has been already conducted in that direction for alumina-based hydrotreating catalysts using γ-Al_2O_3 thin films grown on $MgAl_2O_4$[26,33] Basal-bonded MoS_2 slabs were typically formed on the (111) and (110) planes of this support. Conversely, edge-bonded clusters were found on the (100) γ-Al_2O_3 plane. A transition from edge to basal-bonded MoS_2 was detected on the (100) plane at 773 K sulfidation temperature, suggesting that the chemistry at the interface is not the

sole determinant factor on the orientation of the MoS_2 slabs and the outcome of the molecular-scale description of active phase-support interactions appears multifactorial.[34] Moreover, the precise nature of alumina thin films is still a matter of debate since Kresse *et al.*[35] showed with the help of DFT that their structure and stoichiometry can be very different from γ-Al_2O_3. Bara *et al.*[24] circumvented this issue by using α-Al_2O_3 wafers of various orientations in order to mimic the surface chemistry of γ-Al_2O_3.[24,25] Four different α-Al_2O_3 orientations were used (A$(11\bar{2}0)$, C(0001), M$(10\bar{1}0)$, and R$(1\bar{1}02)$) and their hydroxylated surface structures were compared to the speciation of surface hydroxyls (Al-OH) on γ-Al_2O_3. Extensive experimental and modeling effort has been devoted to the description of the sorption sites on the α-Al_2O_3 C(0001) plane, with predominantly OH groups bridging two 6-fold coordinated aluminums (Al_{6c}-μ_2-OH) that are also present on the (111) facet of γ-Al_2O_3. The structure of the A$(11\bar{2}0)$, M$(10\bar{1}0)$ and R$(1\bar{1}02)$ planes have been less studied and therefore their surface structure is still a matter of debate. Nonetheless, experimental and theoretical studies have been gathered to evidence –OH groups singly, doubly and triply bound to 6-fold Al^{3+} (i.e. Al_{6c}-μ_1-OH, Al_{6c}-μ_2-OH, Al_{6c}-μ_3-OH) on the A$(11\bar{2}0)$ and M$(10\bar{1}0)$ planes which are therefore reminiscent of the (111) and (100) facets of γ-Al_2O_3. Finally, singly coordinated –OH groups on 4-fold aluminum (Al_{4c}-μ_1-OH) are exposed on the R$(1\bar{1}02)$ plane which can model the predominant (110) plane of γ-Al_2O_3. The proposed relationship between α-Al_2O_3 and γ-Al_2O_3 surface structures is schematically depicted in Figure 1. Using this approach, it was suggested that key features of hydrotreating catalysts such as the extent of Mo sulfidation as well as MoS_2 orientation was surface-dependent and controlled by the strength of Mo/alumina interactions that were ranked in the following increasing order C(0001) < A$(11\bar{2}0)$, M$(10\bar{1}0)$ < R$(1\bar{1}02)$. The surface speciation of the different α-Al_2O_3 crystal planes is key to understand the properties of the active phase on such model catalysts.

This work aims at increasing the complexity of the model systems studied previously [24,25] by adding phosphorus in the catalyst composition. This dopant is widely used in industrial formulations since there is general agreement that it leads to an increase in HDS activity[36–42] by reducing the interactions between the active phase and the support as phosphates block the basic surface Al –OH sites that selectively interact with the Mo active phase. It has also been reported that phosphorus can improve Mo dispersion.[43] Nonetheless, this beneficial effect is highly dependent on the P-loading and on the incorporation method. For instance, co-impregnation of phosphorus and metal precursors modifies the chemical structure of the deposited precursor by forming heteropolyanions,[19,38,40] which may have an effect both on Mo dispersion and posterior catalyst activation. On the other hand, prior P-doping of the support influences the acidity of the support.[36,37,44] The effect exerted by phosphorus is most probably surface-dependent, since the interaction of phosphorus with alumina is controlled by the speciation of the alumina sorption sites which are different on each crystal plane (see Figure 1). However, such surface-dependent P-doping has never been investigated in the literature before.

In this work, phosphorus-doped model MoS_2 catalysts supported on four different crystal planes of α-Al_2O_3 C(0001), A$(11\bar{2}0)$, M$(10\bar{1}0)$ and R$(1\bar{1}02)$ were synthesized via spin-coating deposition in order to mimic an aqueous-phase deposition on powder materials while keeping an homogeneous distribution

on planar supports as shown before.[45,46],[47] In order to evaluate the surface-dependent P-doping with various P/Mo ratio, the impregnation solution speciation was studied with liquid-state NMR and the planar catalysts were characterized with XPS and TEM at the oxidic state and after subsequent sulfidation at different temperatures in order to study the effect of phosphorus on Mo dispersion and genesis of the active MoS_2 phase.

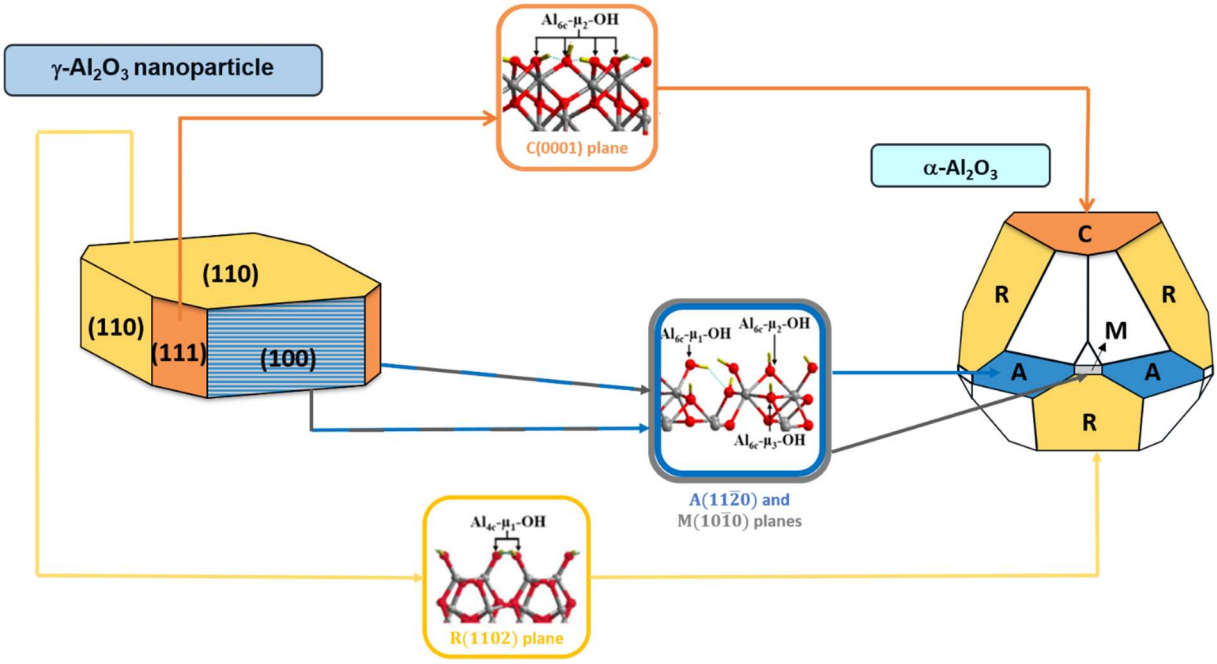

Figure 1. Schematic representation of the proposed relationship [24] between the crystal planes of γ-Al_2O_3 [48] and α-Al_2O_3 [49] through their converging sorption sites.

2. Materials and Methods

2.1 Preparation of model Mo(P) / α-Al_2O_3 catalysts

2.1.1 Model α-Al_2O_3 wafers

The model HDS catalysts synthesized throughout this work were prepared on four different single-crystal planes of α-Al_2O_3 wafers: A$(11\bar{2}0)$, C(0001), M$(10\bar{1}0)$, and R$(1\bar{1}02)$. These substrates are commercially available: the A$(11\bar{2}0)$ and R$(1\bar{1}02)$ single crystals were provided by MaTecK Material Technologie & Kristalle GmbH (Germany), with dimensions 1.0 cm x 1.0 cm x 0.50 mm (thickness). An average rugosity of the crystals of Ra< 0.50 nm was reported by the provider. The C(0001) and M$(10\bar{1}0)$ single crystals were provided by SurfaceNet GmbH (Germany), with the same dimensions as the A$(11\bar{2}0)$ and R$(1\bar{1}02)$ planes. In this latter case, the surface roughness measured in terms of average rugosity was Ra < 0.35 nm according to the specifications of the provider.

A standardized cleaning procedure for the single crystals was adopted as a first synthesis stage in order to limit chemical contamination of the surfaces. The chemical cleaning was carried out prior to every active phase deposition and its methodology was directly adopted from the procedure established by the work of Tougerti *et al.*[50] and Bara *et al.*[25] (successive washings with water, HNO_3 and NH_3). The cleaning step was automatized and was carried out by a synthesis robot (Zinsser Analytic), in order to ensure a fully reproducible initial chemical state for the α-Al_2O_3 wafers. After the cleaning procedure was completed, the crystals were dried under nitrogen flux and subsequently calcined in air at 700 °C for 14 hours inside a muffle oven.

2.1.2 Preparation of the Mo-P precursor solution

The precursor solutions were prepared using MoO_3 (Fluka, >99% purity) as molybdenum source, while the phosphorus source was aqueous H_3PO_4 (Aldrich, >85 %v). Initially, three solutions with different P/Mo molar ratio (0.11, 0.40 and 0.57) were prepared with the same Mo concentration of 0.1 M, according to the protocol described by Costa *et al*.[19,51] A fixed amount of MoO_3 (i.e. 1.439 g of MoO_3 for 100 mL of solution) was dissolved in distilled water. Afterwards, the appropriate volume of H_3PO_4 (for instance, 83 µL for 100 mL of P/Mo = 0.11 solution) was added to the aqueous solution in order to obtain the desired P/Mo molar ratio. The solutions were stirred and refluxed at 90 °C for two hours in order to fully dissolve the Mo and P precursors. The final pH was measured for the three solutions, yielding values of 1.9, 1.8 and 1.8 for the P/Mo = 0.11, 0.40 and 0.57 solutions, respectively. Finally, a solution with P/Mo = 0.57 was also prepared using ammonium heptamolybdate (AHM, Merck, 99% purity) as Mo source following the same protocol as described above with MoO_3. The pH of the latter solution yielded a value of 2.4.

2.1.3 Deposition of the precursor solution via spin-coating

The deposition of the Mo-P precursors was carried out by the spin-coating technique (commercial spin-coater, Süss MicroTec) in which the wafer is rotated at a constant fixed speed during a defined time while the precursor solution falls right above the wafer in motion, as seen in Figure 2. A suction pump conveniently placed under the sample holder creates the necessary vacuum for the wafer to remain in place despite the centrifugal force caused by the rotation. The rotation of the wafer was fixed at 1800 rpm (0.5 second to reach this speed) during 45 seconds. At the start of the rotation, the precursor solution was introduced by a syringe pump (kd Scientific), for a total volume of 150 µL, at a speed of 10 $\mu L.s^{-1}$. These parameters were established empirically in order to obtain a target Mo loading of about 3 $atoms.nm^{-2}$.

After Mo-P deposition, the wafers were directly calcined at 450 °C (without further drying) for two hours in air inside a muffle furnace. The recovered samples are afterwards referred as “oxide state”.

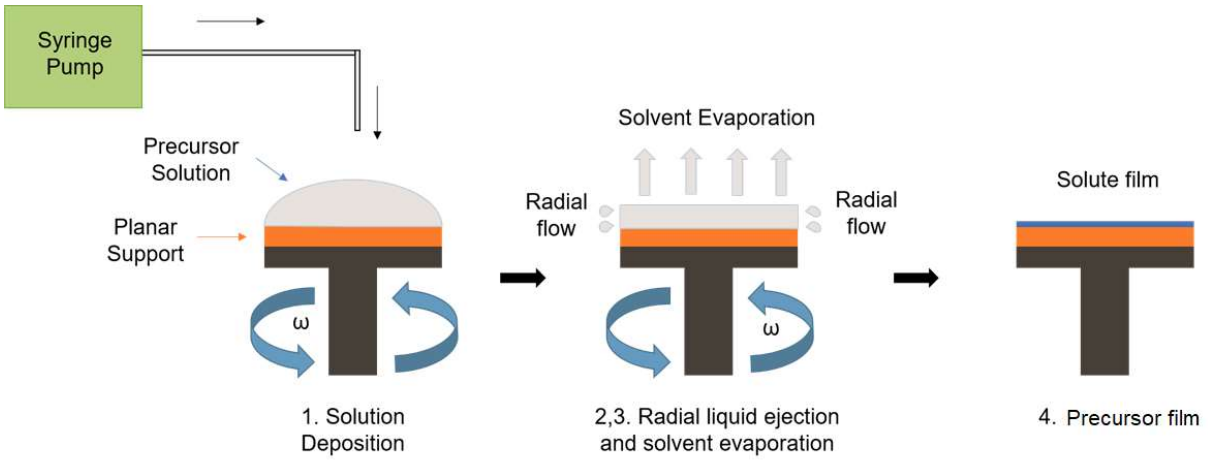

Figure 2. Scheme for the spin-coating deposition of the Mo-P precursor solution.

2.2 Sulfidation of model catalysts

Gas phase sulfidation of the model catalysts was performed in a glass reactor at atmospheric pressure by heating the sample (at 15°C.min^{-1}) under a 2NL·h^{-1} 15 % mol H_2S/H_2 gas flow from room-temperature to the sulfidation temperature ranging from 100 to 500 °C. This temperature was maintained for two hours. After sulfidation, the system was cooled under Ar until 80 °C after the 100 °C sulfidation temperature or until 150 °C for the other sulfidation temperatures, under a 2NL·h^{-1} Ar flow. The system was kept at this temperature for 1 hour in order to desorb the sulfur excess on the surface of the catalysts. The catalysts were then transferred and conserved under Ar atmosphere into a storage recipient filled with Ar before analysis. The recovered samples are afterwards referred as “sulfide state”.

For the sake of clarity, the samples prepared from MoO_3 will be referred to the α-Al_2O_3 crystal plane used as support (A$(11\bar{2}0)$, C(0001), M$(10\bar{1}0)$, and R$(1\bar{1}02)$) followed by the P/Mo ratio of the precursor solution (0.11, 0.40 and 0.57). All samples prepared from ammonium heptamolybdate (AHM) were prepared with a P/Mo ratio of 0.57 and will be denoted plane-AHM. A summary of the respective samples is displayed in Table 1.

Table 1. Summary of the different prepared samples

Mo precursor	MoO_3			AHM
List of Samples	A-0.11	A-0.40	A-0.57	A-AHM
	C-0.11	C-0.40	C-0.57	C-AHM
	M-0.11	M-0.40	M-0.57	M-AHM
	R-0.11	R-0.40	R-0.57	R-AHM

2.3 Nuclear Magnetic Resonance (NMR) analysis of the precursor solutions

Liquid-state ^{31}P NMR spectra were obtained on a Bruker Avance III spectrometer equipped with a BBI 5 mm probe, operating at frequency of 202 MHz. The obtained chemical shifts were calibrated using the signal of 10% H_3PO_4 (0 ppm) as external standard. The sequence 30° with inverse gated decoupling ^{31}P was acquired with a 60s recycle delay and with a ^{1}H decoupling Waltz 16. The number of scans was 1024 with an acquisition time of 1s. The spectra were processed with a zero-filling factor of 1 and with an exponential decay corresponding to a 1 Hz line broadening in the transformed spectra. Only spectra with the same line broadening are directly compared.

Liquid-state ^{95}Mo NMR spectra were also obtained on a Bruker Avance III spectrometer equipped with a BBO low-gamma 10 mm probe, operating at frequency of 39.1 MHz. The obtained chemical shifts were calibrated using the signal of 2M Na_2MoO_4 in D_2O as external standard. The sequence zg 90° ^{95}Mo was acquired with a 1s recycle delay. The number of scans was 21504 with an acquisition time of 1s. The spectra were processed with a zero-filling factor of 2 and with an exponential decay corresponding to a 0 Hz line broadening in the transformed spectra. Only spectra with the same line broadening are directly compared.

2.4 X-ray photoelectron spectroscopy (XPS) analysis of Mo and P

The information of the chemical nature and the surface concentration of the different species in the model catalytic system was obtained by XPS, in both oxide and sulfide states. The XPS spectra were obtained with an Omicron (ESCA+) instrument using a monochromatic Al X-ray source ($h\nu$ = 1486.6 eV) with an accelerating voltage of 14 kV and a current of 20 mA (with an overall energy resolution of 0.8 eV). The spectra were collected at a takeoff angle of 90° under a pressure below $1 \cdot 10^{-9}$ mbar at ambient temperature. The analyzed area is about 1 mm^2 and three different spots were analyzed for each sample. The quantitative results are the average of the three analyses for each sample. In order to obtain high-resolution spectra, the analyzer operated at an energy of 20 eV for the selected elemental scanning and 100 eV for the overall elemental survey. The scans were performed using a 0.1 eV step over the selected elements. The surveyed regions were C1s, O1s, Al2p, Mo3d, P2p and S2p. The obtained spectra for each scanned region were calibrated based on adventitious carbon, which is independent of the nature of the surface being analyzed. In that sense, the C1s photopeak was established at 284.6 eV, following the premises of Gandubert *et al.*[52,53] An electron flood-gun was required in order to ensure the charge neutralization of the alumina substrate as it is an insulating material that will undergo surface charging upon ejection of the photoelectrons. After spectra collection, the mathematical decomposition of the different contributions was performed using the Casa XPS software.[54] The decomposition of the obtained spectra was carried out using Gaussian-Lorentzian functions, while the background subtraction was Shirley-type.

The surface density (in atoms·nm^{-2}) of molybdenum and phosphorus was calculated for each planar catalyst according to the quantification model used by Tougerti *et al.*[50] derived from the work of Towle *et al.*[55] The expression for Mo surface density (respectively phosphorus) is given by:

$$[\mathrm{Mo\ or\ P}]_{\mathrm{surface}} = \frac{\mathrm{A_{Mo3d}}\ \sigma_{\mathrm{Al2p}}\ 2\rho_{\mathrm{Al2O3}}}{A_{\mathrm{Al2p}}\ \sigma_{\mathrm{Mo3d}}\ \mathrm{MW_{Al2O3}}} \cdot \lambda_{\mathrm{Al}} \qquad (1)$$

Where A_{Mo3d} (respectively A_{P2p}) and A_{Al2p} are the total areas of the Mo3d (respectively P2p) and Al2p XPS photopeak regions, σ_{Al2p} and σ_{Mo3d} (σ_{P2p}) are the photoionization cross sections (0.441 for Al, 8.19 for Mo and 1.0095 for P), ρ_{Al2O3} and MW_{Al2O3} are the density and molar mass of α-Al_2O_3 (3.95 g·cm^{-3} and 102 g·mol^{-1}). λ_{Al} is the average mean free path of Al photoelectrons in Al_2O_3 (3.28 nm[56]).

The Mo3d XPS spectra of sulfided Mo-based catalysts can be decomposed into three contributions: MoO_3, MoO_xS_y and MoS_2. By expressing the total Mo surface density as a sum of the areas corresponding to the three Mo contributions, it is possible to express the relative percentage of MoS_2 with respect to the rest of Mo species, as shown in the following expression:

$$\%\ \mathrm{MoS_2} = \frac{\mathrm{A_{MoS_2}}}{\mathrm{A_{MoS_2}} + \mathrm{A_{MoO_xS_y}} + \mathrm{A_{MoO_3}}} \times 100 \qquad (2)$$

$\%MoS_2$ will be referred hereto as sulfidation degree. Sulfided samples were transferred from the storage recipient filled with Ar to the XPS vacuum chamber in air in less than ten seconds. It was duly checked that the sulfidation degree was not modified by the transfer procedure.

2.5 Transmission Electron Microscopy (TEM)

TEM samples were obtained by scraping the surface of the model Mo(P) / α-Al_2O_3 catalysts with a stainless steel razor blade in order to obtain fragments of the model samples thin enough to carry out transmission electron microscopy. The detached fragments were suspended into a drop of absolute ethanol, which was then deposited on a carbon-coated Cu-grid for TEM analysis. Conventional TEM images were collected with a JEOL 2010 microscope operating at 200 kV. The average MoS_2 slab length and stacking number were obtained by measuring no less than 220 clusters per sample, using the ImageJ 1.45 software.[57] The slab length for each MoS_2 slab was obtained by manually measuring the visible blackened stripes that contrasted with the lighter α-Al_2O_3 background. The stacking number was determined by quantification of visible stripe layers for every MoS_2 cluster.

3. Results

3.1 Speciation of Mo-P precursor solutions

3.1.1 ^{31}P NMR of MoO_3-based solutions

Mixed molybdate-phosphate precursor solutions were prepared from MoO_3 and H_3PO_4 (Mo concentration of 0.1 M). It is known[19,40,51,58–60] that this type of composition will lead to a variety of Mo-containing compounds, including predominantly phospho-molybdic heteropolyanions (HPA). In order to address the speciation of the impregnation solutions, liquid-state ^{31}P and ^{95}Mo NMR was carried out for the three solutions with varying P/Mo ratio (P/Mo = 0.11, 0.40 and 0.57).

The quantitative ^{31}P NMR spectrum for each solution is shown in Figure 3. ^{31}P NMR analysis first strongly suggests that all phosphorus in solution is detected (no precipitation for example), since the relative total peak area (Σ peaks on the figure normalized to the P/Mo = 0.11 case) is in agreement with the P/Mo ratio introduced in the solution.

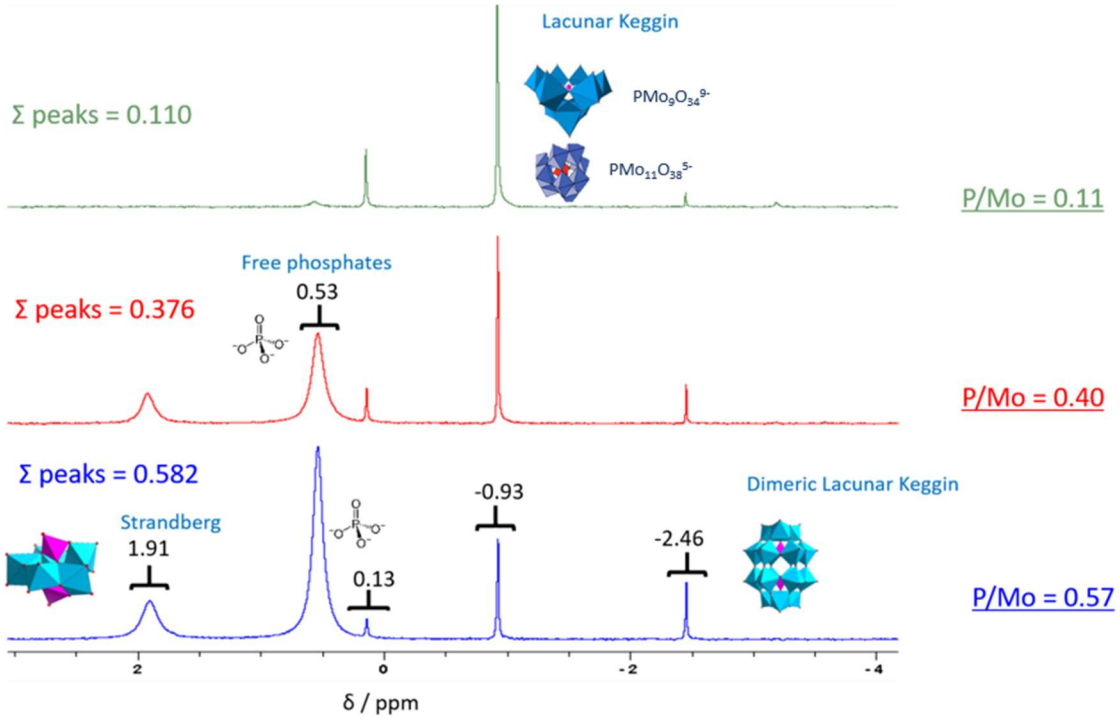

Figure 3. Quantitative liquid-state ^{31}P NMR spectra of the P/Mo 0.11, 0.40 and 0.57 solutions prepared with MoO_3 as molybdenum source (Mo concentration of 0.1 M) and H_3PO_4 as phosphorus source. The measured solution pH was 1.9, 1.8 and 1.8 respectively. Peak chemical shifts are indicated in black. Σ peaks was normalized to the P/Mo = 0.11 spectrum for the sake of clarity. Schematic representation of

phospho-molybdic HPA are also shown (molybdenum octahedra in blue and phosphorus tetrahedra in pink).

In order to ascribe the peaks observed in Figure 3, a summary of different phospho-molybdic species and their respective ^{31}P chemical shifts reported in the literature is given in Table 2.

Table 2. Reported ^{31}P NMR chemical shifts for various phospho-molybdic species according to different sources using H_3PO_4 85 wt% as standard.

	δ /ppm			
Reference	Griboval *et al.*[61]	Pettersson *et al.*[58,62]	Kraus and Prins[63]	van Veen *et al.*[60,64]
Phosphates	0.5	0.48	0.5*	0.5
$P_2Mo_5O_{23}^{6-}$	2.0	1.86 to 2.35 *	2.0	2.0 to 2.3 *
$PMo_9O_{34}^{9-}$	-0.9	-1.15 to -1.00 *	-	-1.1 to 0.9 *
$P_2Mo_{18}O_{62}^{6-}$	-2.5	-2.53	-	-2.4
$PMo_{11}O_{38}^{5-}$	-	-1.2 to -0.78 *	-	-1.14 to 0.9 *
$PMo_{12}O_{40}^{3-}$	-	-3.2	-	-3.2

*The range corresponds to different protonation degrees

According to Table 2, phosphate groups should appear at around 0.5 ppm on the NMR spectra. However, pH variations, as well as partial protonation may displace this chemical shift. It should be kept in mind that this pH dependence on the chemical shift also applies for phospho-molybdic HPA, as shown by van Veen *et al*.[60] Therefore, small variations of their NMR position (shown as a chemical shift range in Table 2) is observed depending on the solution pH.

It can be noted in Figure 3 that increasing phosphorus contents in solution (e.g. higher P/Mo) leads to a notorious increase in the broad signal at 0.53 ppm (free phosphates) and for P/Mo = 0.57, free phosphates become, by large, the predominant phosphorus species. Therefore, ^{31}P NMR results show that high phosphorus content in solution necessarily implies a large excess of free phosphates in such solution.

According to Table 2, the signal at δ = -0.93 ppm present in the three spectra displayed in Figure 3 can be attributed to a lacunar Keggin $PMo_9O_{34}^{9-}$ species (chemical shift from -0.9 to -1.15 ppm,[61–64] depending on its protonation degree). Moreover, the peak at -0.93 ppm is predominant for the P/Mo = 0.11 solution (Fig. 3, green) which is in good agreement with a P/Mo stoichiometry of 0.11 for the $PMo_9O_{34}^{9-}$ HPA. However, according to literature data (Table 2), this signal could also correspond to $PMo_{11}O_{38}^{5-}$. Hence, it is not possible to discriminate both species based on their chemical shift only and the signal at δ = -0.93 ppm is assigned to both species in Figure 3.

In all solutions, a peak of varying intensity is also observed at a chemical shift of -2.46 ppm that can be attributed to a dimeric Keggin structure $P_2Mo_{18}O_{62}^{6-}$ HPA, since the values of chemical shift for this species reported in Table 2 range from -2.45 to -2.53 ppm.

At high phosphorus content in solution (from P/Mo = 0.40), a rather broad signal appears at a chemical shift of 1.91 ppm, ascribed to the Strandberg-type HPA $P_2Mo_5O_{23}^{6-}$ according to Table 2, and in agreement with the P/Mo ratio for this HPA (P/Mo = 0.40). This change in the speciation with increasing P content is also in concordance with the chemical equilibria proposed by Iwamoto and Grimblot[39] involving $P_2Mo_5O_{23}^{6-}$:

$$(44 - 14x)\,H^+ + 5\,Mo_7O_{24}^{6-} + 14\,H_xPO_4^{3-x} = 7\,H_2P_2Mo_5O_{23}^{4-} + 15\,H_2O \qquad (2)$$

$$(13x - 18)H^+ + 15\,H_2O + 9\,H_2P_2Mo_5O_{23}^{4-} = 5\,PMo_9O_{34}H_6^{3-} + 13\,H_xPO_4^{3-x} \quad (x > 1) \quad (3)$$

In both equations, an increasing concentration of free phosphates will displace the equilibrium towards the formation of the P_2Mo_5 Strandberg-type HPA.

The presence of a minor signal at 0.13 ppm should be noted as well. Pettersson *et al.*[58] suggested that this species corresponded to a PMo_9-like isomer and established its range of chemical shift between 0.47 and 0.08 ppm. Alternatively, van Veen *et al.*[60] suggested that this species was a PMo_6-type heteropolyanion without firmly concluding. Either way, these previous studies strongly support the hypothesis that this species is a phospho-molybdic HPA.

Finally, a very weak signal corresponding to the $PMo_{12}O_{40}^{6-}$ HPA is observed for the P/Mo = 0.11 solution at around -3.2 ppm. This signal completely disappears at higher phosphorus contents.

In order to evaluate the effect of the Mo source on the speciation of the precursor solution, a solution prepared with ammonium heptamolybdate (AHM) instead of MoO_3 with a P/Mo = 0.57 was characterized by ^{31}P NMR. The natural (i.e. as prepared) pH of both solutions is noticeably different: 1.8 for the MoO_3-based solution and 2.4 for the AHM-based solution. Hence, a third solution synthesized from MoO_3 was pH-corrected to 2.4 with NH_4OH in order to match the AHM condition. The obtained spectra are displayed in Figure 4.

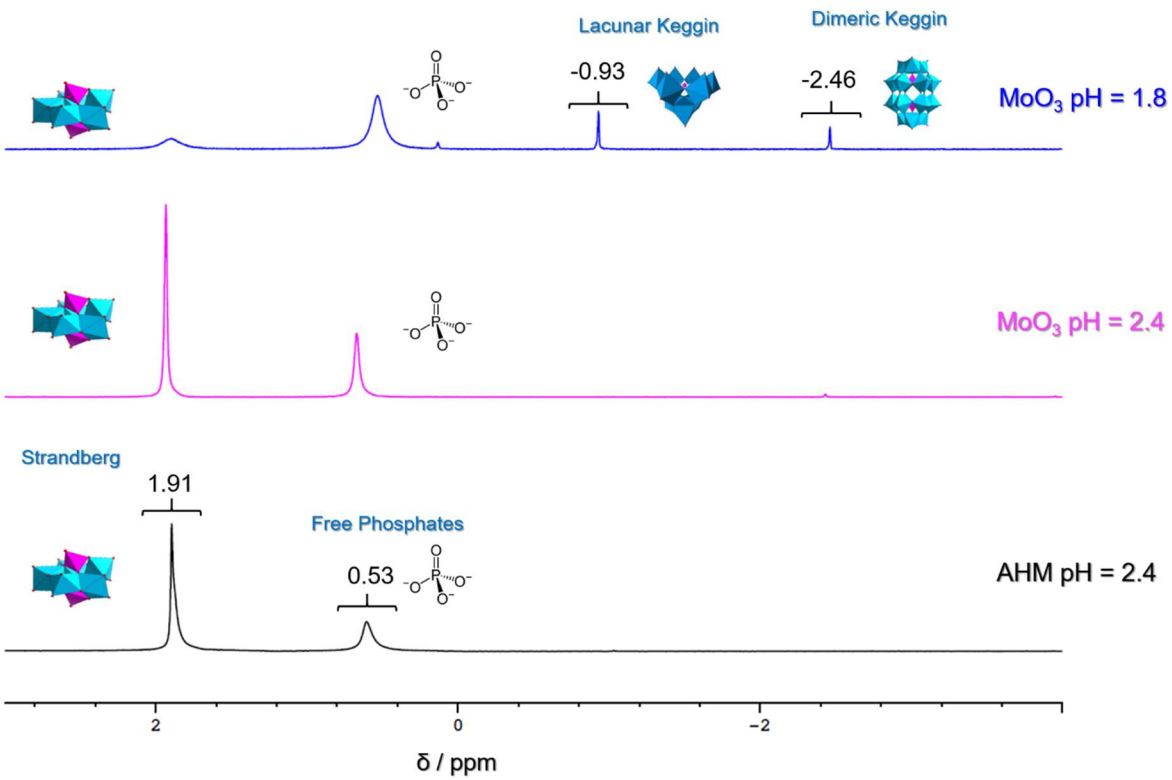

Figure 4. Quantitative liquid-state ^{31}P NMR spectra of a P/Mo = 0.57 solution prepared : i) from MoO_3 with its intrinsic pH (blue, pH = 1.8), ii) from MoO_3 after correcting the pH (pink, pH = 2.4) and iii) from AHM (black, pH = 2.4) as molybdenum sources and H_3PO_4 as phosphorus source.

As seen in Figure 4, the speciation of phosphorus-containing species prepared from AHM as Mo source (pH = 2.4) is much simpler than for MoO_3 with its intrinsic pH (i.e. 1.8). In the former case, only the $P_2Mo_5O_{23}^{6-}$ Strandberg-type structure and free phosphates are found in solution. In addition, the amount of free phosphates in solution drastically decreases under these conditions. Such an influence of the Mo source cannot have a kinetic origin since Hervé *et al.*[65] showed that (poly)molybdates have a low kinetic stability and a thermodynamic equilibrium should be reached whatever the Mo source. As a matter of fact, when correcting the pH of the MoO_3 solution to 2.4 (Figure 4, pink) the same speciation of phospho-molybdic species is observed with MoO_3 and AHM. Therefore, the solution pH (i.e. thermodynamic parameter) is the driving force that will determine the phospho-molybdic speciation in solution rather than the molybdenum source. The lower pH destabilizes Strandberg species in favor of Keggin type HPAs.

The integration of the different peaks shown in Figure 3 and Figure 4 allows one to obtain a relative percentage of each species for the four precursor solutions at their natural pH (Table 3).

Table 3. Relative proportion (in % of the total area of the NMR spectrum) of each species in the different precursor solutions at their natural pH (Mo concentration of 0.1 M). The $H_xPO_4^{x-3}$

concentration marked with an asterisk indicate the free phosphate concentration in solution calculated from the initial P concentration and the relative proportion of free phosphates.

Species	Precursor solution			
	P/Mo = 0.11 (MoO_3)	P/Mo = 0.40 (MoO_3)	P/ Mo = 0.57 (MoO_3)	P/ Mo = 0.57 (AHM)
H_xPO_4 $^{x-3}$	9 (0.001 mol·L^{-1})*	59 (0.02 mol·L^{-1})*	67 (0.04 mol·L^{-1})*	37 (0.02 mol·L^{-1})*
$PMo_{12}O_{40}$ $^{3-}$	3	-	-	-
$P_2Mo_{18}O_{62}$ $^{6-}$	4	3	3	-
PMo_9O_{34} $^{9-}$ and/or $PMo_{11}O_{39}$ $^{7-}$	69	13	6	-
Undefined HPA	15	4	2	
$P_2Mo_5O_{23}$ $^{6-}$	-	21	22	63

*Undefined HPA refers to the peak at 0.13 ppm previously reported by Pettersson *et al.*[58,62] and van Veen *et al.*[66]

For the MoO_3-based solution, and the lowest P/Mo ratio (P/Mo = 0.11), 91% of all phosphorus atoms are incorporated into phospho-molybdic HPA while 9% remain as free phosphates. This tendency is reversed after increasing the P/Mo ratio in solution to and above 0.40. Phosphorus is now mainly present as free phosphates (about 70% of phosphorus species for P/Mo = 0.57 at the natural pH of 1.8). Conversely, for the solution prepared from AHM at P/Mo = 0.57 (pH = 2.4), the amount of free phosphates is below 40%.

The most important conclusion that can be drawn from the liquid-state ^{31}P NMR study of the four solutions is that the speciation of the phosphorus-containing species can be controlled by playing both with the initial P/Mo ratio and with the Mo precursor, while keeping the natural pH of the solution which is typically the case in catalyst preparation. At low P/Mo ratios (i.e. 0.11), the impregnation solution contains mostly phospho-molybdic HPA (75 %) while at high P/Mo ratio (i.e. 0.57) free phosphates are the predominant species (70 %) for MoO_3-based solutions. Solutions prepared from AHM at P/Mo = 0.57 show a considerably reduced amount of free phosphates.

3.1.2 ^{95}Mo NMR of MoO_3-based solution

The composition of the impregnation solution was also studied through liquid-state ^{95}Mo NMR in order to a have a more comprehensive view of the Mo speciation.

Whatever the Mo source (in absence of phosphorus), the stable Mo oxo-species in concentrated solution and acidic pH such as those used in the present study is the heptamolybdate ion: $Mo_7O_{24}^{6-}$. This structure shows three non-equivalent MoO_6 octahedra and its ^{95}Mo NMR spectrum is expected to exhibit three different signals. In fact, several authors[67–69] report these three contributions, schematized in Figure 5 along with their chemical shifts: a small signal at a chemical shift of 210 ppm (green), and two overlapping contributions at 32 (blue) and 15 (red) ppm. The monomolybdate MoO_4^{2-}, if present, would yield a signal at 0 ppm since it is the reference used for ^{95}Mo NMR.

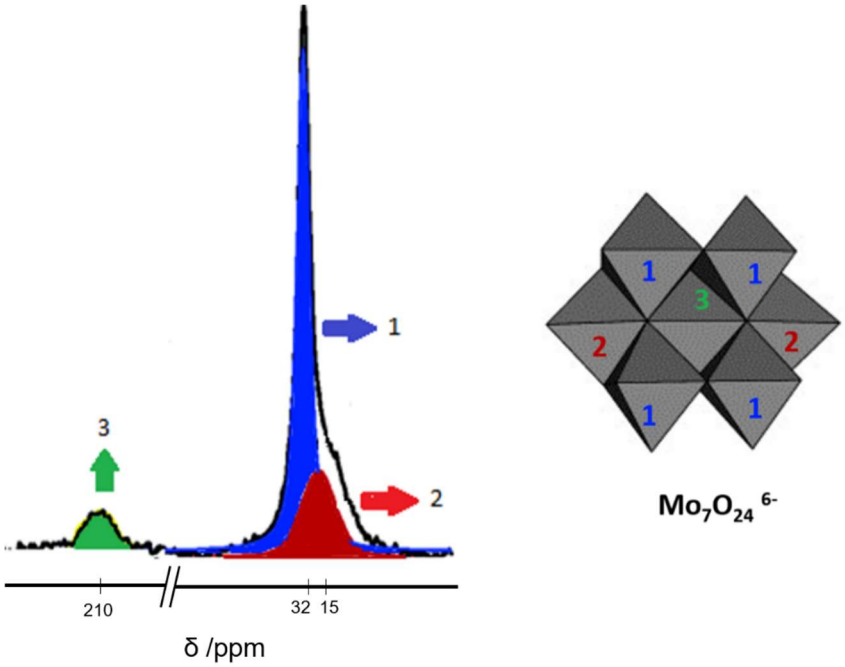

Figure 5. Different ^{95}Mo NMR signals attributable to the $Mo_7O_{24}^{6-}$ polyanion. Adapted from Fedotov *et al.*[67]

For the $P_2Mo_5O_{23}^{6-}$ Strandberg-type structure, Fedotov *et al.*[67,70] report a chemical shift ranging from -18 to -11 ppm, depending on the protonation degree.

Concerning the $PMo_9O_{34}^{9-}$ lacunar Keggin structure, no information is reported in the literature regarding its ^{95}Mo NMR signal to the best of our knowledge. However, a chemical shift of -34/-35 ppm is reported for $P_2Mo_{18}O_{62}^{6-}$ [69,70]. Since the structure of this dimeric $P_2Mo_{18}O_{62}^{6-}$ HPA is made of two $PMo_9O_{34}^{9-}$ lacunar Keggin units, the Mo octahedra share the same electronic environment in both species and the chemical shift for the monomeric $PMo_9O_{34}^{9-}$ structure should approach the one of the dimeric. In that sense, a signal for the lacunar $PMo_9O_{34}^{9-}$ Keggin structure appearing at around -30 ppm will overlap with the corresponding Strandberg-type signal.

A summary of different phospho-molybdic species and their respective ^{95}Mo chemical shifts reported in the literature is given in Table 4.

Liquid-state ^{95}Mo NMR was carried out for the three different precursor solutions (P/Mo = 0.11, 0.40 and 0.57) prepared from MoO_3, in order to confirm the different contributions identified with ^{31}P NMR, and to detect the possible presence of free molybdates ($Mo_7O_{24}^{6-}$ and MoO_4^{2-}). The spectra for the three different solutions are displayed in Figure 6.

Table 4. Reported ^{95}Mo NMR chemical shifts for various phospho-molybdic species using Na_2MoO_4 2M as standard.

	δ /ppm		
Reference	Fedotov *et al.*[67,70]	Maksimovskaya *et al.*[68]	Kazansky[69]
$Mo_7O_{24}^{6-}$	15, 34, 210	34, 200-210	-
$P_2Mo_5O_{23}^{6-}$	-18 to -11*	-	-
$P_2Mo_{18}O_{62}^{6-}$	-34	-	-35
$PMo_{12}O_{40}^{3-}$	16	-	22

*The range corresponds to different protonation degrees

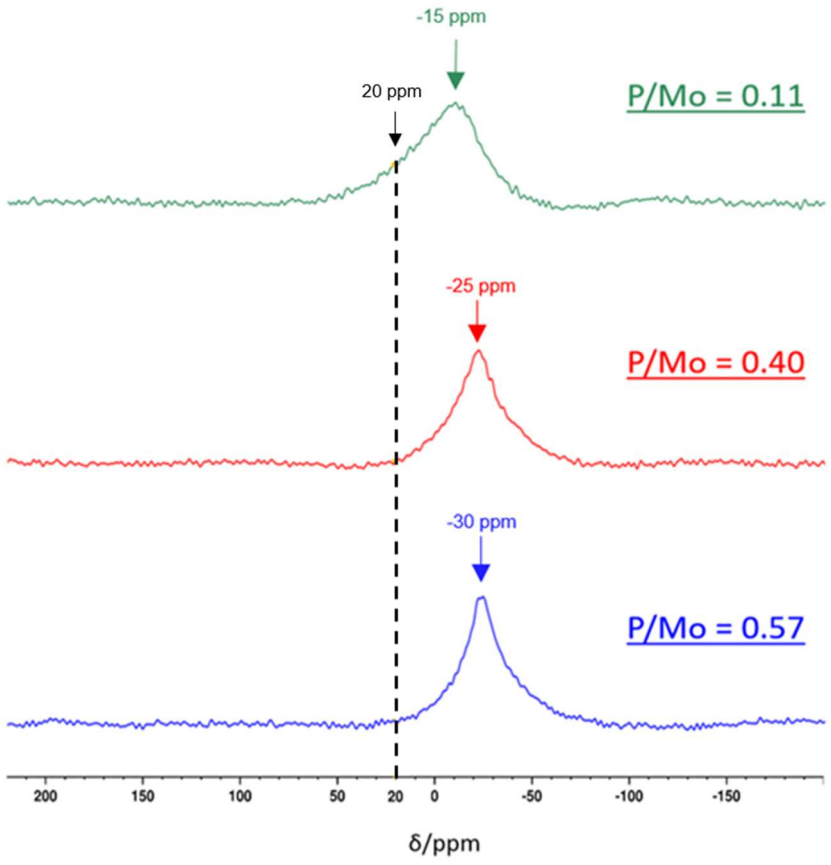

Figure 6. Liquid-state ^{95}Mo NMR spectra of the P/Mo = 0.11, 0.40 and 0.57 solutions prepared with MoO_3 as molybdenum source and H_3PO_4 as phosphorus source. The reference (0 ppm) is a 2 M solution of Na_2MoO_4.

For the P/Mo = 0.11 solution (green), a predominant broad signal pointing at -15 ppm is observed along with a shoulder at about 20 ppm. The main maximum can be assigned to the monomeric $PMo_9O_{34}^{9-}$ or $PMo_{11}O_{39}^{7-}$ lacunar Keggin structures in agreement with the ^{31}P NMR (Figure 3). The shoulder at about 20 ppm suggests the presence of free heptamolybdates in solution. In this case, the signal at 210 ppm referenced in Figure 4 would be too weak to be detected. For the P/Mo = 0.40 and 0.57 solutions, one

more symmetric signal is observed at around -25/-30 ppm. This unique signal may be the result of the superposition of the ^{95}Mo NMR contributions of both lacunar Keggin $PMo_9O_{34}^{9-}$ and Strandberg-type $P_2Mo_5O_{23}^{6-}$ HPA, which were detected via ^{31}P NMR. The signal at -25/-30 ppm becomes more symmetric and narrower when increasing the P/Mo ratio in line with the decreasing contribution of $PMo_9O_{34}^{9-}$ HPA (Table 3). More importantly, for these two solutions, the absence of a shoulder-type contribution at around 20 ppm suggests the absence of free heptamolybdates for these solutions.

The ^{95}Mo NMR spectrum of the solution prepared from AHM (Figure 7) shows a symmetric signal centered at around -20 ppm in full agreement with the ^{31}P NMR spectrum (Figure 4) showing only one phospho-molybdic species, the Strandberg-type P_2Mo_5 HPA. The presence of free heptamolybdates (~20 ppm) can be excluded. The slight downfield shift observed for the AHM-based solution with respect to the solution prepared from MoO_3 may be explained either by different pH in both solutions (2.4 and 1.8 respectively), or by the remaining PMo_9 and P_2Mo_{18} species in MoO_3-based solutions that may overlap with the predominant P_2Mo_5 HPA.

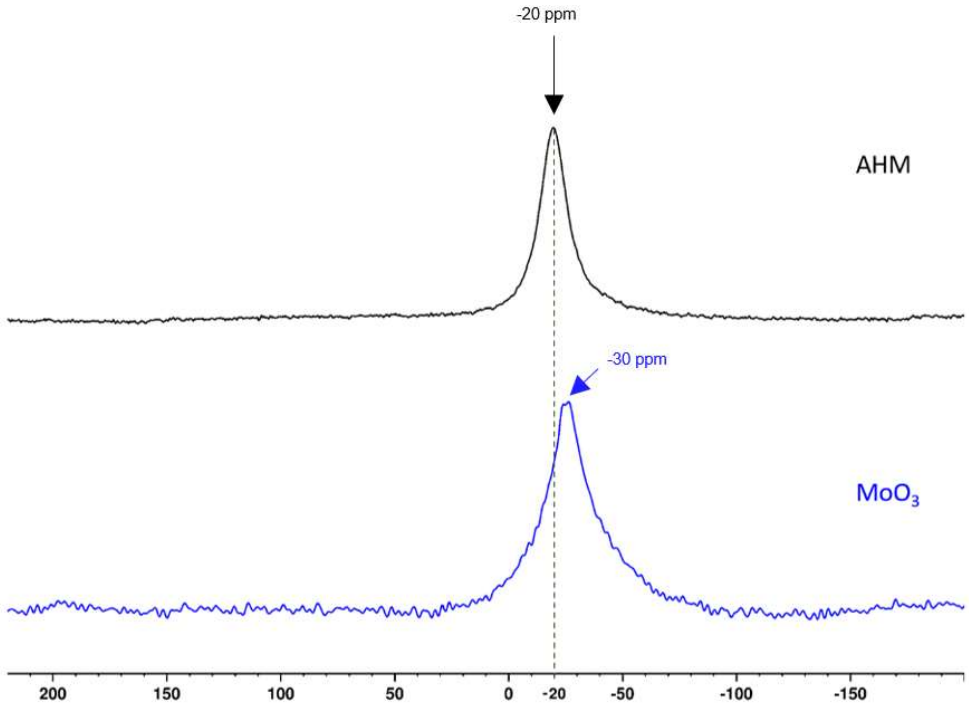

Figure 7. Liquid-state ^{95}Mo NMR spectra of the P/Mo = 0.57 solution prepared from AHM (black, pH = 2.4) and MoO_3 (blue, pH = 1.8) as molybdenum sources and H_3PO_4 as phosphorus source.

All the obtained liquid-state ^{31}P and ^{95}Mo NMR spectra allow us to conclude that the speciation of the Mo-P impregnation solution depends both on the Mo source and the phosphorus loading if no pH regulation is performed:

- For MoO_3 as Mo source, a low P/Mo ratio in solution (0.11) will yield a solution with mostly phospho-molybdic HPA (mainly lacunar Keggin PMo_9) and a minor amount of free phosphates, and free molybdates (most probably as heptamolybdates).
- For MoO_3 as Mo source, the P speciation for a high P/Mo ratio in solution (0.57) will yield a solution with a predominant contribution of free phosphates and a minor contribution of HPA.
- Changing the Mo source to AHM instead of MoO_3, and keeping a high P/Mo ratio (0.57) significantly changes the speciation of the solution with a predominant contribution of HPA (Strandberg P_2Mo_5) and a low amount of free phosphates.

Hence, the relative proportion of phospho-molybdic HPA and free phosphates can be finely tuned by playing with the P content and Mo source.

3.2 Spin-coating of a pure phosphate solution on α-Al_2O_3 wafers

In order to better understand the interactions between phosphate and alumina, we first study the deposition of phosphates on the different α-Al_2O_3 crystal planes. A spin-coating deposition experiment was carried out on the four crystal planes (A$(11\bar{2}0)$, C(0001), M$(10\bar{1}0)$, and R$(1\bar{1}02)$) using a pure phosphate solution (0.057 M phosphoric acid, pH adjusted to 1.8 with ammonium hydroxide). The chosen concentration corresponds to the one for a solution with P/Mo = 0.57 used for P-doped-model catalysts, which will be discussed below. The results of the surface atomic P/Al ratio obtained from XPS analysis are displayed in Figure 8. The surface phosphorus densities obtained from these results (see Equation 1) are available in Figure S.1 of Supporting Information.

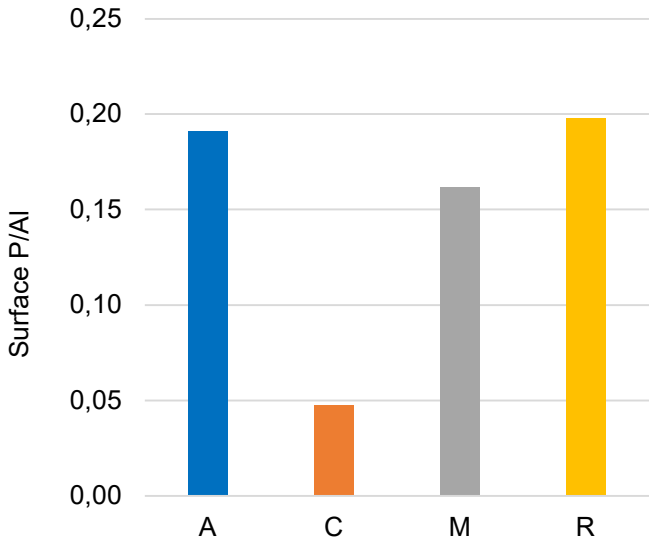

Figure 8. Surface atomic phosphorus/aluminum ratio obtained with XPS on the A$(11\bar{2}0)$, C(0001), M$(10\bar{1}0)$ and R$(1\bar{1}02)$ crystal planes of α-Al_2O_3 after spin-coating deposition of a phosphate solution. The samples were analyzed after calcination at 450 °C.

The results in Figure 8 indicates a higher surface P/Al ratio on the A($11\bar{2}0$) and R($1\bar{1}02$) planes (ca. 0.20), a much lower ratio (ca. 0.05) on the C(0001) plane and an intermediate behavior for the M($10\bar{1}0$) plane. These results pinpoint either a surface selectivity in the dispersion of the phosphate species on the different crystal planes or a selective adsorption during spin-coating deposition. In Figure S.1 (Supporting Information), the calculated P surface densities follow the same trend. It should be noticed that these latter values are especially higher than those achieved by traditional wet impregnation method: a 5 wt% P_2O_5 containing HDT catalyst (assuming a specific area of 280 m^2/g) correspond to less than 1 atoms $P.nm^{-2}$. This can indicate that we are beyond a phosphorus monolayer. Next, such differences between faces can hardly be explained by a selective adsorption of phosphates on the surface since spin-coating is very close to a mere physical deposition on the surface (this will be confirmed below for phosphomolybdate solutions). A more probable explanation for this selectivity is a different phosphate aggregation on the surface (which can vary with the nature of the interactions between these groups and the surface sorption sites). Different phosphate aggregation states can alter the XPS quantification. Formation of large phosphate clusters dispersed on the surface should lead to an attenuation of the P_{2p} signal and consequently to an underestimation of P/Al. This tendency of phosphate groups to aggregate into polyphosphate clusters has been already observed.[71] Conversely, the presence of small phosphate clusters covering the surface will lead mainly to an attenuation of the Al_{2p} signal and in turn to an overestimation of P/Al on the surface. This analysis also holds for the calculations of P surface densities reported in Figure S1 since the model used for the determination of P surface loadings (see experimental section) implies that the mean free path of Al_{2p} photoelectrons and P_{2p} in the sorbed phase (3.2 nm[56]) is much larger than the thickness of the sorbed phase (phosphates), which would correspond to a homogenous and monolayer phosphate deposition. Such hypothesis is no longer valid when there is surface aggregation (clustering) of the supported phase and results of Figure S1 have to be taken as a qualitative guide only.

Hence, results of Figure 8 lead to the hypothesis of large phosphate clusters dispersed on the C(0001) plane (lower P dispersion) while small particles would cover the whole surface on the R($1\bar{1}02$) plane, increasing P dispersion. Figure 8 can thus be used to rank the α-Al_2O_3 crystal planes in terms of phosphate aggregation: C(0001) >> M($10\bar{1}0$) > A($11\bar{2}0$), R($1\bar{1}02$). Figure 9 gives a schematic view of this conclusion. It can be concluded that phosphates interact differently with each crystal plane, which would certainly play a role in the deposition of phospho-molybdic precursors, especially at high phosphate contents in solution.

Moreover, these results are also in line with our previous work on molybdate deposition where it was demonstrated that the C(0001) plane induced weak metal-support interactions leading to molybdate aggregation. Smaller particles were obtained on the R($1\bar{1}02$) plane indicating stronger metal-support interactions. An intermediate and similar behavior was obtained with the A($11\bar{2}0$) and M($10\bar{1}0$) planes that exhibit comparable surface structure. Very similar conclusions can be drawn from Figure 8 for phosphates except from a distinct behavior for the A($11\bar{2}0$) and M($10\bar{1}0$) planes. In the latter case, phosphate deposition appears more sensitive than molybdate regarding the surface chemistry but the

present knowledge of the surface structure of both orientations does not allow us to rationalize this behavior.

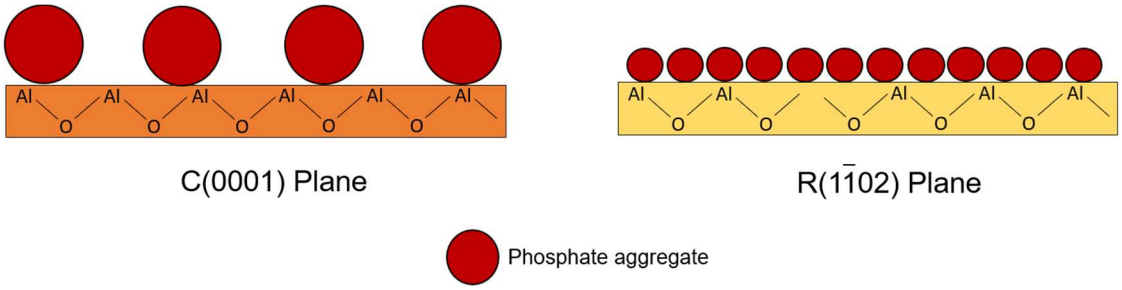

Figure 9. Schematic representation of the dispersion of phosphate groups on the C(0001) and R(1$\bar{1}$02) planes of α-Al_2O_3.

3.3 Spin coating of phospho-/molybdic solutions with varying P/Mo ratios and Mo sources on α-Al_2O_3 wafers

Model catalysts were then prepared by spin-coating the Mo-P precursor solutions characterized in Section 3.1 on the four different α-Al_2O_3 crystal planes. XPS was also used to quantify their surface P/Mo atomic ratio in the oxide state (after calcination at 450°C) and the results are displayed in Figure 10.

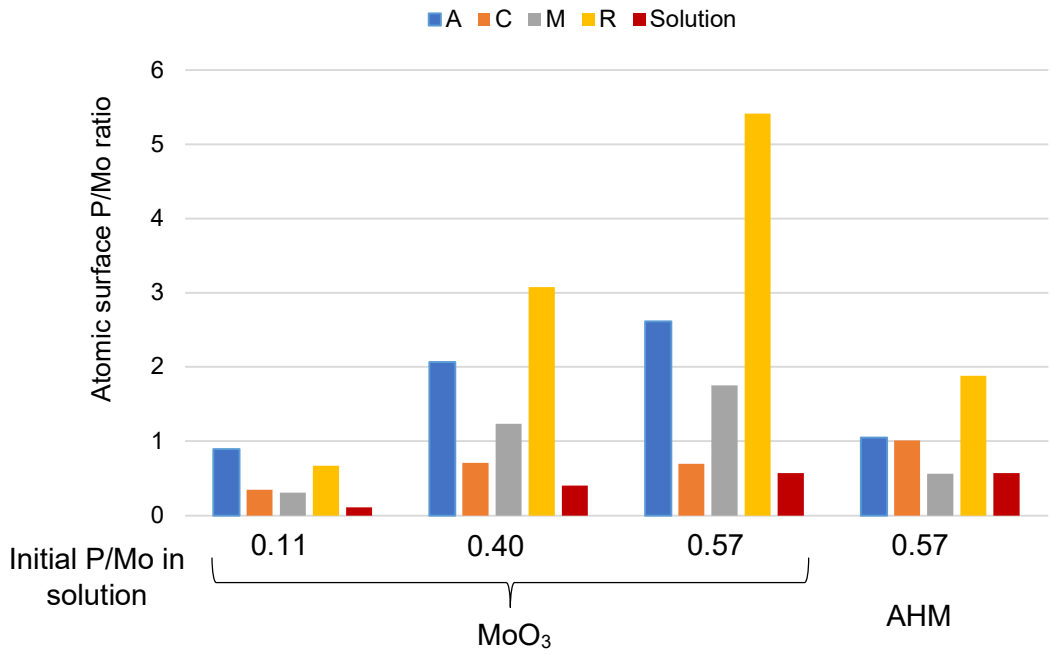

Figure 10. Average P/Mo atomic ratio obtained with XPS for the model catalysts in oxide state (calcined at 450°C/2h) for different precursors solutions (MoO_3 or AHM based) with varying initial P/Mo

ratio, supported on the A(11$\bar{2}$0), C(0001), M(10$\bar{1}$0) and R(1$\bar{1}$02) crystal planes of α-Al_2O_3. The red bar gives the P/Mo ratio in solution. The average corresponds to three different samples per crystal plane and precursor solution.

Firstly, it is worth noticing that regardless of the phosphorus content in the precursor solution, the analyzed P/Mo atomic ratio on the surface is always higher than the initial P/Mo ratio in such solutions (red bar). Another clear behavior shown in Figure 10 is the strong dependence of the surface P/Mo atomic ratio with the α-Al_2O_3 crystal plane which is reminiscent of the results for pure phosphate solutions (Figure 8). This selectivity is better evidenced at high initial P/Mo ratio in solution. The same trend is obtained when plotting P/Al instead of P/Mo (see Figure S.2 of supporting information) since the former ratio is often used as a descriptor of dispersion.[19]

As discussed in the previous section, this selectivity can most probably be explained by different aggregation states on the surface. In order to discard a selective adsorption of P or Mo which is unlikely with spin-coating, a comparative impregnation experience was carried out where a controlled amount of Mo and P was drop casted on the α-Al_2O_3 wafers. Two impregnation solutions were chosen with P/Mo = 0.57 and prepared from MoO_3 and AHM by dilution of the mother spin-coating solutions to $6.6 \cdot 10^{-6}$ mol·L^{-1} for a target Mo loading of 4 atoms·nm^{-2}. XPS quantification of the P/Mo ratio (See Figure S.3 of supporting information) show that the surface selectivity observed in Figure 10 is maintained after drop-casting, while a complete control of Mo and P loading should lead to identical surface P/Mo ratio, whatever the considered face. Hence, selective deposition of P vs. Mo can be discarded, while surface-dependent aggregation is a more plausible hypothesis to explain the various P/Mo ratio on the different crystal planes of α-Al_2O_3.

In order to discuss more precisely the evolution of the P/Mo ratio, the average surface atomic Mo/Al ratio obtained by XPS is reported in Figure 11. In general, there is a tendency toward the decrease of the Mo/Al ratio for the same surface orientation upon increasing phosphorus concentration in the precursor solution, i.e. increasing initial P/Mo ratio. The type of Mo precursor (MoO_3 or AHM) does not drastically alter the measured Mo loading. The only exception for this is the C(0001) plane at P/Mo = 0.11. However, variations of Mo/Al (Figure 11) are much smaller than variations of P/Mo (Figure 10). Figure S.4 (Supporting Information) displays the Mo loading (in atoms.nm^{-2}) calculated from Equation 1. In this case, the Mo surface concentration ranges from 1.5 to 4.5 atoms·nm^{-2}, which would correspond to weight loadings from 6 to 17 wt% Mo for a conventional catalyst supported on a powder γ-Al_2O_3 carrier of about 280 m²/g (these values are also on the same order of magnitude than Mo surface concentrations encountered in HDT catalysts).

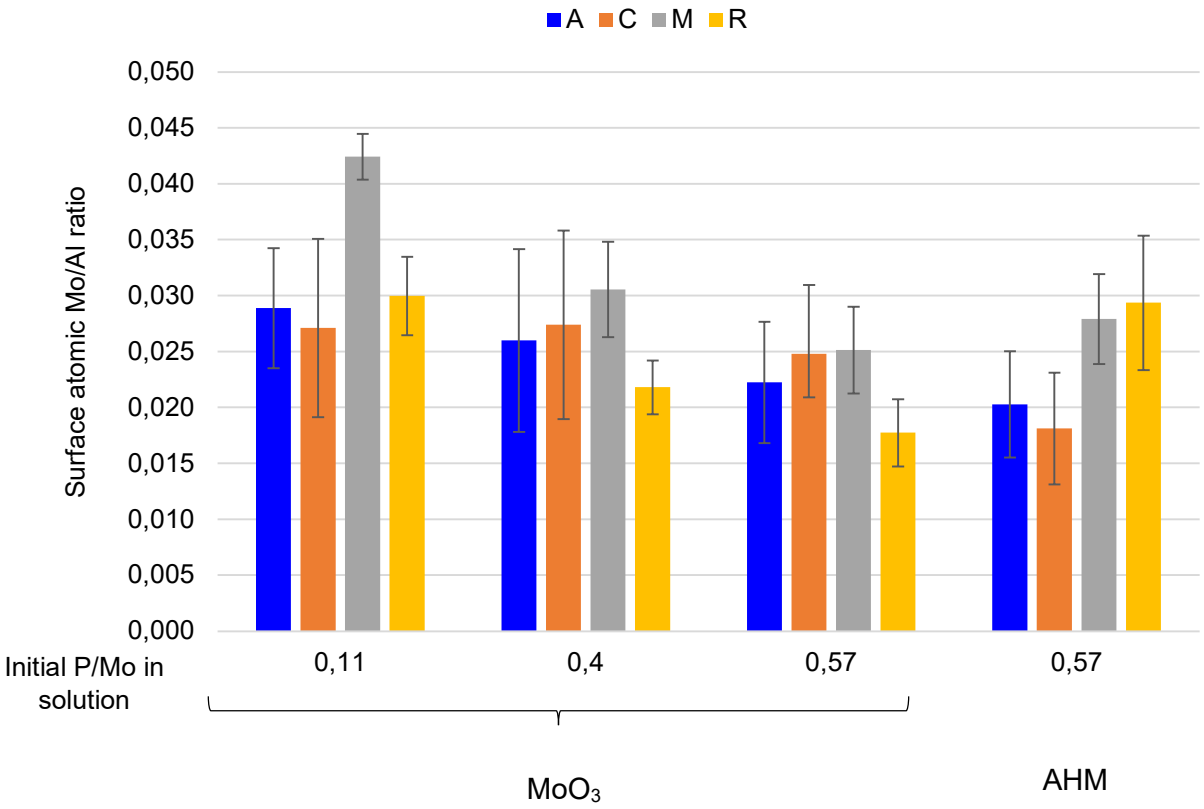

Figure 11. Average surface atomic Mo/Al ratio (2-3 samples each) obtained by XPS for the model Mo-P/ α-Al_2O_3 catalysts in oxide state (calcined at 450°C/2h) for different precursor solutions (MoO_3 or AHM) with varying initial P/Mo ratio, supported on the A(11$\bar{2}$0), C(0001), M(10$\bar{1}$0) and R(1$\bar{1}$02) α-Al_2O_3 crystal planes. Error bars give the standard deviation obtained on 2-3 samples.

Combining the results of Figures 10 and 11, the large variation of P/Mo ratio observed on each α-Al_2O_3 surface orientation can be related mainly to variations of the P quantification (as already observed on Fig. 8), rather than to the Mo one, which shows weaker fluctuations with the type of α-Al_2O_3 facets. Moreover, it was suggested above that the P/Al ratio (Figure S.2 and consequently the surface P/Mo ratio, Figure 10) can be used as a descriptor of the surface-dependent phosphate aggregation. In line with the results of Fig. 8 (pure phosphate adsorption), it can be concluded that low P/Mo ratio indicates an underestimation of P loading explained by phosphate aggregation (typically, the C(0001) plane). Conversely, a high P/Mo ratio suggests a high surface coverage with small phosphate clusters (typically the R(1$\bar{1}$02) plane). P/Mo ratio can also be seen as an indicator of the P dispersion onto the surface.

It can also be noticed that the apparent surface-dependence of P/Mo is linked to the solution composition (initial P/Mo ratio and type of Mo precursor), which can be correlated to the solution speciation (see section 3.1). At low initial P/Mo ratios (e.g. 0.11), a weak variation of the surface P/Mo ratio can be linked to a low amount of free phosphates in solution as shown by ^{31}P NMR (see Figure 2). At higher initial P/Mo ratios (0.40 and 0.57-MoO_3), a strong surface-dependence is observed, which is in line with a large amount of free phosphates in solution (Figure 2). Moreover, it is interesting to compare the model catalysts prepared from MoO_3 and AHM as Mo source for the same initial P/Mo ratio. In both solutions,

the speciation of the precursor differs significantly (Figure 3), with a much larger amount of free phosphates for MoO_3-based solutions. According to Figure 10, model catalysts prepared from the latter solution show a much larger surface-dependent P/Mo ratio than for AHM-based, where the R($1\bar{1}02$) plane is the only surface that stands out noticeably. This variation with the type of Mo precursor confirms that the surface-dependent P/Mo ratio can be correlated to the amount of free phosphates in the impregnation solution: the higher the relative phosphate proportion in solution with respect to HPA, the higher the P/Mo surface dependence. As for the type of surfaces involved, Figure 10 shows that planes A($11\bar{2}0$) and R($1\bar{1}02$) show a much higher atomic surface P/Mo ratio than the C(0001) and M($10\bar{1}0$) planes for the same initial P/Mo ratio. These results are somehow in line with the results displayed in Figure 7 for the phosphate loading.

Hence, all these results converge to show that the presence of free phosphate groups in solution affects the apparent surface P/Mo ratio on the different crystal planes which is used as a descriptor of the surface aggregation. Therefore, phosphates adsorbed on the A($11\bar{2}0$) and R($1\bar{1}02$) planes are much more dispersed than in the case of the C(0001) plane, which would tend to favor bigger phosphate aggregates whereas the M($10\bar{1}0$) plane shows an intermediate behavior.

These conclusions are in line with the works of van Veen *et al*.[64] and Bergwerff *et al*.[72], who observed a strong and preferential adsorption of phosphate groups on powder γ-Al_2O_3 with respect to Mo-P HPA. -Phosphate adsorption on surfaces that exhibit strong metal-support interactions (A$(11\bar{2}0)$ and R$(1\bar{1}02)$ planes) will lead to small phosphate clusters while weakly interacting surfaces (C(0001) plane) will promote phosphate aggregation upon calcination. These differences are much less pronounced when there is a reduced fraction of free phosphates in solution (AHM-based solutions or low P/Mo ratio).

As for Mo, phosphate adsorption will reduce the sorption sites for Mo.[72] In fact, van Veen *et al*.[64] suggested that for P loadings higher than 0.3 wt%, $AlPO_4$ layers can build up on the surface of the support, blocking the strongest adsorption sites from Mo precursors. This newly-formed $AlPO_4$ layer has a lower adsorption capacity than the original γ-Al_2O_3 support. This can explain why the total apparent Mo content (Fig. 11) decreases with the increase of initial P/Mo since consumption of sorption sites will cause the aggregation of Mo.

3.4 Genesis of the active (sulfide) phase

The genesis of the active phase in HDT catalysts consists in the transformation of the oxidic precursor into MoS_2 nanoclusters (active phase) via H_2S/H_2 sulfidation. It has been shown by several authors that the extent of this sulfidation is support and surface dependent[24,73,74], since the temperature at which the MoO_x clusters will be transformed into MoS_2 depends on the support. The sulfidation degree is then a direct indicator of the strength of the active phase-support interactions: higher sulfidation degrees obtained at lower temperatures imply weaker metal/support interactions.[75] The presence of phosphorus

can intervene in the evolution of the sulfidation trend, since it can affect Mo-O-Al interactions by blocking Mo adsorption sites,[76,77] by playing a role on the acidity of the support,[37,38] or by intervening directly in the architecture of the MoS_2 phase.[44,78] Moreover, we have shown above that phosphorus doping is also dependent on the alumina surface orientation since XPS demonstrated a surface-dependent aggregation of phosphates on the various α-Al_2O_3 wafers investigated.

All synthesized model Mo-P/α-Al_2O_3 catalysts were sulfided at different temperatures (100 to 500 °C) in order to evaluate the evolution of the sulfidation degree (% MoS_2) within this temperature range. The quantification of the sulfidation degree was performed via decomposition of the XPS signals for the different Mo and S contributions according to the procedure described by Bara *et al.*[25] (see experimental section).

3.4.1 Catalysts prepared using the P/Mo = 0.11 precursor solution

The sulfidation trend for the model catalysts prepared using the P/Mo = 0.11 solution is displayed in Figure 12.

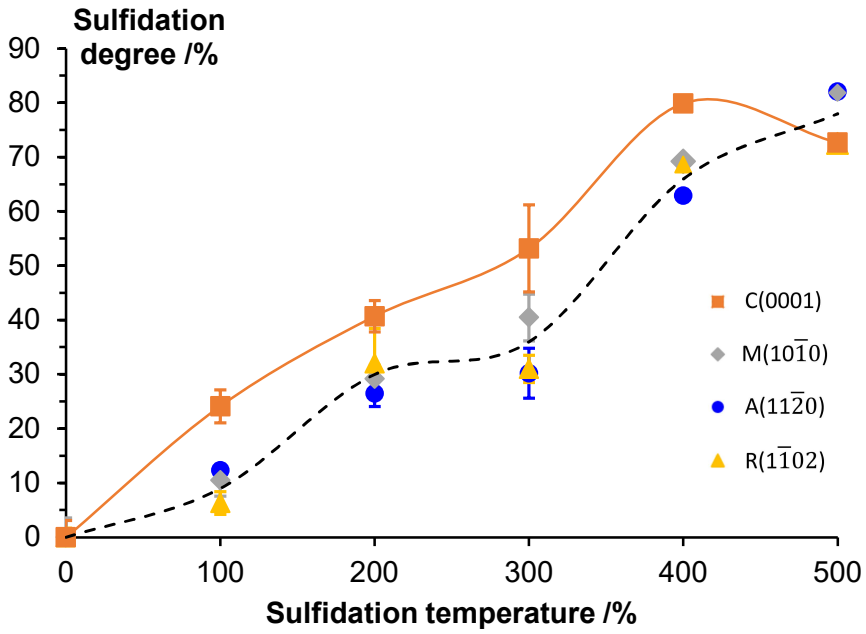

Figure 12. Sulfidation degree (% MoS_2) determined via XPS at different temperatures of model Mo-P/α-Al_2O_3 catalysts prepared using the P/Mo = 0.11 phospho-molybdic solution (from MoO_3) on the C(0001), A(11$\bar{2}$0), M(11$\bar{1}$0) and R(1$\bar{1}$02) planes of α-Al_2O_3. Note: at 500 °C, results for planes A and M are superposed, as well as for planes C and R. The continuous orange line corresponds to the trend followed by the model catalysts prepared on the C(0001) plane, while the black dotted one corresponds to a general trend for the model catalysts supported on the other crystal planes.

For all model catalysts prepared with the P/Mo = 0.11 precursor solution, sulfidation started around 100 °C. At this temperature, it is manifest that the catalyst on the C(0001) plane of α-Al_2O_3 is more

sulfided (sulfidation degree of 24%) than the rest of the catalysts on the other crystal planes (sulfidation degree between 6-10%). This is in agreement with the work of Bara *et al.*[24], in which model catalysts (without phosphorus) supported on the C(0001) plane consistently exhibited higher sulfidation degrees, especially at low sulfidation temperatures. The enhanced sulfidation degree on the C(0001) plane is maintained up to 400 °C, reaching a maximum value of around 80% in agreement with what is found for powder catalysts.[53] In that sense, the observed trend in sulfidation for low P-doped catalysts is the same as for non-doped MoS_2 catalysts[24] which means that low P loadings have no significant effect on the sulfidation of Mo oxides.

3.4.2 *Catalysts prepared using the P/Mo = 0.57 precursor solution from MoO_3.*

In the case of the catalysts prepared with the highest P loading (P/Mo = 0.57, MoO_3), the trends for the sulfidation degree for such model system are displayed in Figure 13.

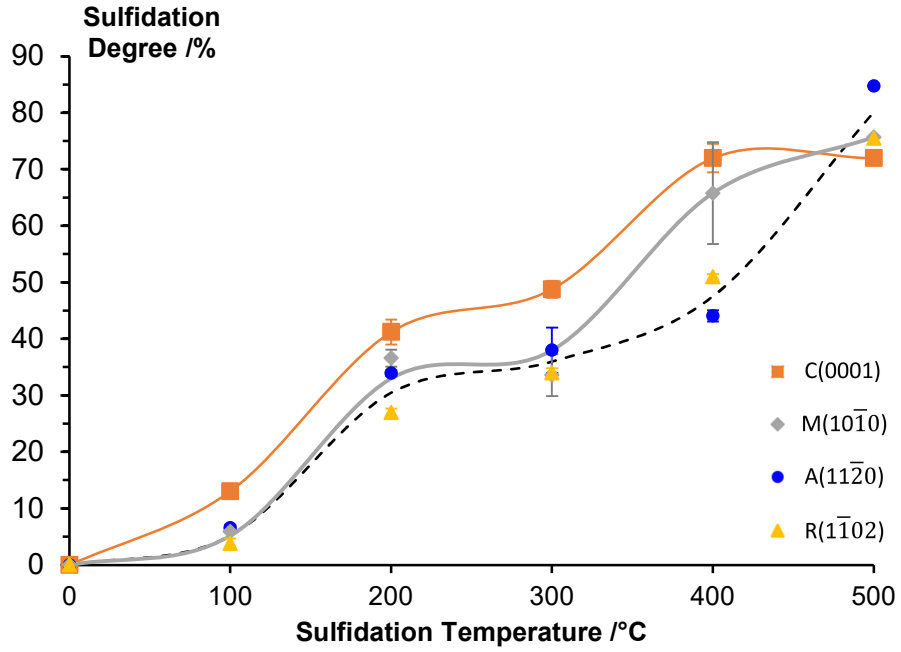

Figure 13. Sulfidation degree determined via XPS at different temperatures of model Mo-P/α-Al_2O_3 catalysts prepared using the P/Mo = 0.57 phospho-molybdic solution (from MoO_3), deposited on the C(0001), A(11$\bar{2}$0), M(10$\bar{1}$0) and R(1$\bar{1}$02) planes of α-Al_2O_3 . The continuous orange and grey lines correspond to the trends followed by the model catalysts prepared on the C(0001) and M(10$\bar{1}$0) planes respectively, while the black dotted one corresponds to a general trend for the catalysts supported on the A(11$\bar{2}$0) and R(1$\bar{1}$02) crystal planes.

Figure 12 shows that for high initial P/Mo ratio, the C(0001) plane always exhibits higher sulfidation degree up to 400°C (even if the 200 °C temperature is less clear-cut). The 300 and 400°C temperatures are also interesting since a change in the trend is observed. At 300°C, the situation observed for the

P/Mo = 0.11 condition still holds: sulfidation is higher on the C(0001) plane (49%) while the other A(11$\bar{2}$0), M(10$\bar{1}$0) and R(1$\bar{1}$02) orientations are lower and close (34-38 %). Conversely, at 400 °C sulfidation for the M(10$\bar{1}$0) plane (66%) is very close to that of the C(0001) plane (72%) while the A(11$\bar{2}$0) and R(1$\bar{1}$02) planes remains less sulfided (44-51%). Sulfidation at higher temperatures (500°C) levels out for all orientations except for the A(11$\bar{2}$0) plane. Hence, three different behaviors for high initial P/Mo ratio can be highlighted and are marked as trendlines in Figure 13: i) a constantly higher sulfidation degree exhibited by plane C(0001), a constantly lower sulfidation degree exhibited by planes A(11$\bar{2}$0) and R(1$\bar{1}$02) and an intermediate sulfidation degree for plane M(10$\bar{1}$0).

It is interesting to compare these results of sulfidation with the surface P/Mo ratio reported in Figure 10 for initial P/Mo = 0.57 in solution. Planes A(11$\bar{2}$0) and R(1$\bar{1}$02) show a remarkable delay in the evolution of the sulfidation degree with respect to the C(0001) plane and Figure 10 shows that the former surface have the highest surface P/Mo ratio. The M(10$\bar{1}$0) plane shows an intermediate sulfidation behavior with a lower sulfidation degree with respect to the C(0001) plane up to 300°C and it shows an intermediate P/Mo ratio in Figure 10.

Hence, the progress of sulfidation degree with the temperature can be directly correlated with the surface P/Mo ratio given by XPS. It was suggested above that the surface P/Mo can be used as a descriptor of the phosphate aggregation: high surface P/Mo implying small phosphate clusters covering the surface. In that sense, the results discussed above allow us to propose that small phosphate aggregates will decrease the sulfidation degree progress of planes A(11$\bar{2}$0) and R(1$\bar{1}$02), especially at low sulfidation temperatures.

To better illustrate the phosphorus effect, the sulfidation degrees of model catalysts supported on the R(1$\bar{1}$02) plane, which is the surface leading to the highest surface P/Mo ratio (see Fig. 10, MoO_3), are displayed in Figure 14 (with varying initial P/Mo ratio).

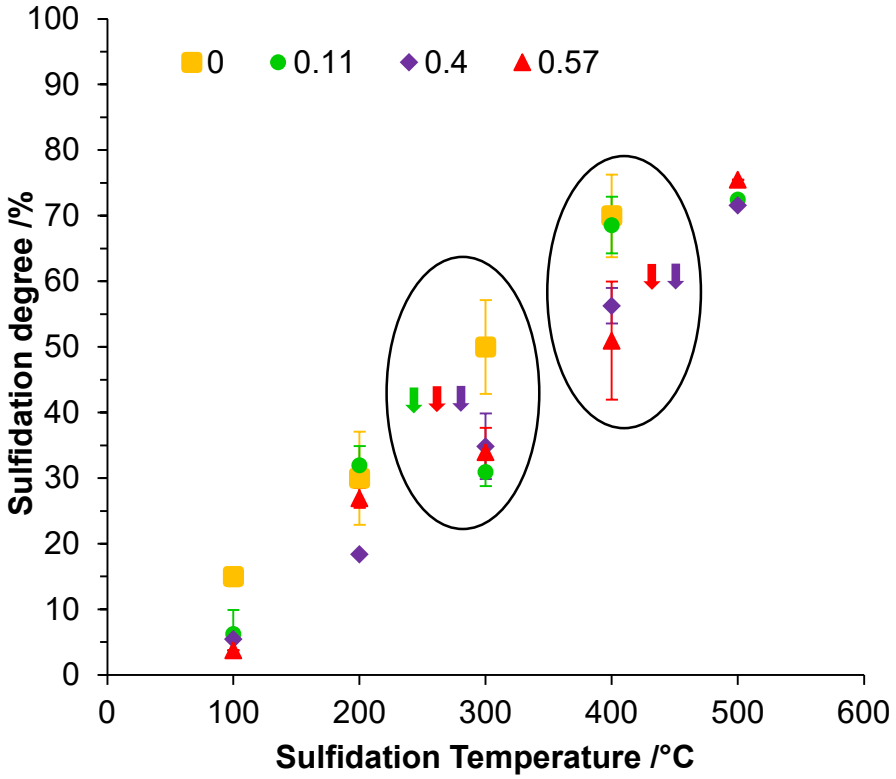

Figure 14. Sulfidation degree determined via XPS at different temperatures of model Mo-P/α-Al_2O_3 catalysts prepared with phospho-molybdic solution (from MoO_3) of varying initial P/Mo ratio on the R($1\bar{1}02$) plane of α-Al_2O_3. The P-content is expressed as initial P/Mo ratio (see Fig. 10). Data points for a P/Mo = 0 correspond to the sulfidation degrees obtained by Bara *et al.*[24] via classical impregnation, as the Mo loadings are comparable with the ones in this work. The enclosed areas mark the delaying phenomena at 300 and 400 °C sulfidation.

Once gain the most striking differences are observed between 300 and 400°C. At 300°C, there are two groups of results: the larger sulfidation (50%) is observed without phosphorus while lower sulfidation (31-34%) is observed in the presence of phosphorus whatever the P/Mo ratio. This demonstrates again the delaying effect of phosphorus upon sulfidation. At 400°C, the inhibition is broken for a low initial P/Mo ratio (0.11) with a sulfidation of 69% identical to the case without phosphorus, while a much lower sulfidation of 51-56% is achieved for catalysts with higher P/Mo (0.40 and 0.57). At 500 °C, the differences are again leveled out since all results converge to a similar sulfidation degree (75%).

3.4.3 Comparison of the catalysts prepared using MoO_3, and AHM as Mo source using a P/Mo = 0.57 precursor solution

Catalysts prepared using the P/Mo = 0.57 precursor solution with AHM as Mo source are useful for comparison with the ones prepared from MoO_3, since i) the AHM-based phospho-molybdic solution shows a reduced number of free phosphates (Figure 3) and ii) the use of AHM-based solutions leads to a lower surface P/Mo ratio (Figure 10). The comparison of both sets of catalysts can give direct

information of the effect of the presence of free phosphates in solution. The sulfidation trends for model catalysts prepared on the A(11$\bar{2}$0) and R(1$\bar{1}$02) planes (i.e. those with the highest surface P/Mo ratio) are displayed in Figure 15.

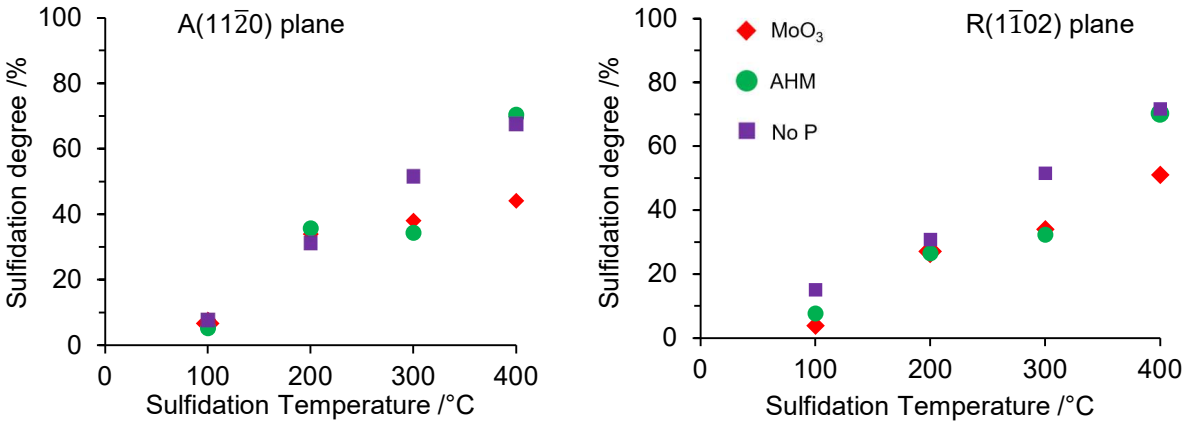

Figure 15. Sulfidation degree determined via XPS at different temperatures of model Mo-P/α-Al_2O_3 catalysts prepared using two phospho-molybdic precursor solutions with an initial P/Mo molar ratio of 0.57 using either MoO_3 or AHM as Mo source and compared to one precursor solution (AHM) without phosphorus, reported by Bara *et al.*[24] deposited on the A(11$\bar{2}$0) (left) and R(1$\bar{1}$02) (right) planes of α-Al_2O_3.

As can be seen from Figure 15, sulfidation is delayed at 300 °C for model catalysts prepared on both crystal planes from phosphorus-containing AHM and MoO_3 precursor solutions (red and green) with respect to a non-doped solution (purple). However, at 400 °C, for both A(11$\bar{2}$0) and R(1$\bar{1}$02) orientations, the catalysts prepared using AHM join the same trend as the non-doped catalysts while the inhibition is still observed for the catalyst prepared with MoO_3. These results confirm the previous conclusions drawn above. A delay in sulfidation takes place whatever the surface P/Mo ratio as long as phosphorus is present but a higher delay (i.e. at higher temperature) is observed for high surface P/Mo ratio (lower clustering) resulting from the presence of a high amount of free phosphates characteristic of MoO_3-based solution with respect to AHM-based solutions. This delay is only overcome at sulfidation temperatures high enough (500°C, Figure 14) to provide the sufficient energy for leveling out different metal-support interactions.

3.4.4 Stacking number measurements via TEM analysis

TEM analyses of the model catalysts in the sulfide state were carried out in order to obtain information about the support effect on the stacking of MoS_2 slabs under the presence of varying phosphorus loadings. The model catalysts used for TEM analysis were sulfided at 400°C, since this is the temperature showing the largest differences in sulfidation degrees among samples (see Fig. 12-15)

besides being a very usual sulfidation temperature. The average stacking distribution of MoS_2 nanoclusters obtained via analyses of the TEM images of model catalysts (Figure 16) is displayed in Figure 17 for the catalysts prepared with low (P/Mo = 0.11) and high (P/Mo = 0.57) P content in solution (from the MoO_3 precursor).

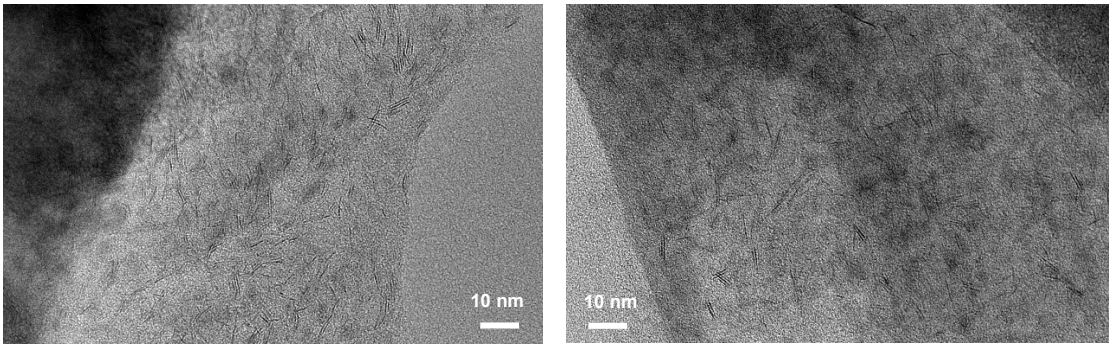

Figure 16. Representative TEM images of model P-doped MoS_2 catalysts supported on the M(10$\bar{1}$0) plane of α-Al_2O_3. Left: low P-content (initial P/Mo = 0.11), Right: high P-content (initial P/Mo = 0.57)

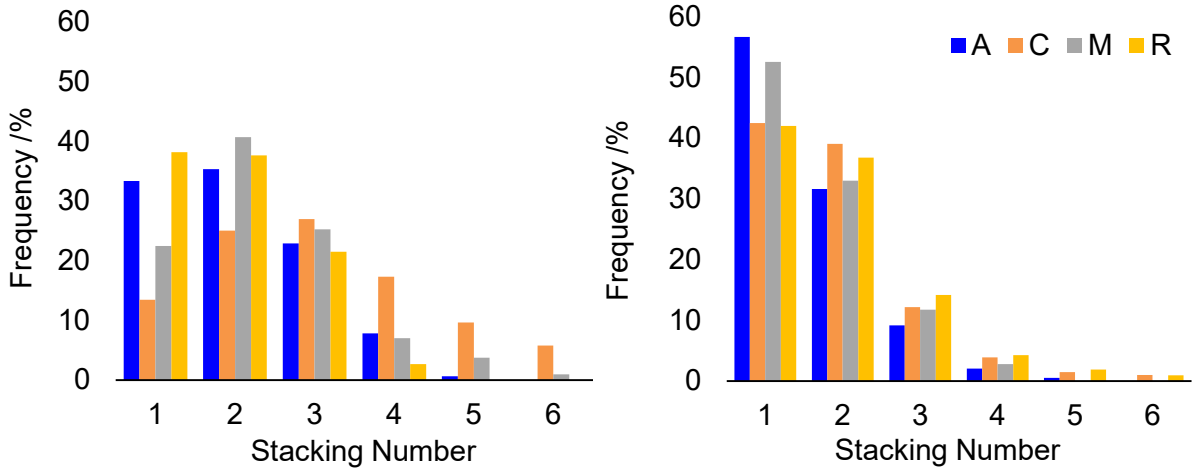

Figure 17. MoS_2 average stacking number for model P-doped MoS_2 catalysts supported on the C(0001), A(11$\bar{2}$0), M(10$\bar{1}$0) and R(1$\bar{1}$02) planes of α-Al_2O_3, prepared with the P/Mo = 0.11 (left) and P/Mo = 0.57 (right) precursor solutions from MoO_3 and sulfided at 400 °C.

First, it can be noted that the average stacking number (Table 5) for model catalysts prepared with a low P content in solution is higher than for those prepared with a higher P content for all crystal planes, which demonstrates a key role of phosphorus.

Table 5. Average stacking number for model catalysts supported on the A($11\bar{2}0$), C(0001), M($10\bar{1}0$) and R($1\bar{1}02$) planes of α-Al_2O_3 prepared with the P/Mo = 0.11 and 0.57 precursor solutions.

P/Mo in solution	A($11\bar{2}0$)	C(0001)	M($10\bar{1}0$)	R($1\bar{1}02$)
0.11	2.0	3.0	2.3	1.9
0.57	1.6	1.9	1.6	1.8

Second, for the model catalysts prepared with the P/Mo = 0.11 solution, MoS_2 slabs on the C(0001) plane show a slightly higher stacking (about three slabs) than on the other planes where the distribution is centered on two slabs. These results go in line with the two distinctive tendencies for sulfidation trends discussed from Figure 12 where the C(0001) plane showed a unique and higher sulfidation degree. A higher stacking for the C(0001) plane was also demonstrated in the absence of P.[24]

In the case of the model catalysts prepared from the P/Mo = 0.57 solution, a clear reduction in the stacking for all the model catalysts is observed since single-slabs are predominant. Hansen *et al*.[79] showed with in-situ TEM that multi-layered MoS_2 slabs grow through an homogenous nucleation of mobile Mo species on top of previously formed single-layered MoS_2 particles. In the present case, it can be assumed that in the presence of phosphorus aggregates, migration of mobile Mo species is constrained leading to a diffusion-limited growth whatever the α-Al_2O_3 orientation. It has also to be noted that the size of the slabs is almost constant for all orientations (i.e. about 4,2 ± 0,9 nm, see Figure S.5 of supporting information).

Conversely, for conventional powder catalysts, it has been found that incorporating phosphorus tend to slightly increases the average MoS_2 stacking number.[39,80] Hence, the results presented here may be specific to planar surfaces where porosity is absent.

4. Discussion: the role of phosphorus on Mo adsorption and genesis of the active phase

Liquid state ^{31}P NMR show that Mo is mainly incorporated in phospho-molybdic HPA while the amount of free phosphates increases with the initial solution P/Mo ratio. XPS quantification of the model catalysts in their oxide state shows a strong surface-dependence of the surface P/Mo ratio: we demonstrate that this strong dependence is a descriptor of the surface aggregation of phosphates. The nature of the substrate (crystal plane), in conjunction with the amount of free phosphates in solution, are the determining factors in this aggregation state.

Our results (Figure 7) show also that the phosphate aggregation is strongly dependent on the strength of surface/adsorbate interaction, as shown before for molybdate adsorption.[25] Phosphates aggregation

decreases in the following order C(0001) >> M$(10\bar{1}0)$ > A$(11\bar{2}0)$, R$(1\bar{1}02)$ with the least interacting surface (C plane) leading to the larger phosphate clusters.

Since phosphates and (heteropoly)molybdates are both oxoanions, they compete for the alumina sorption sites (-OH_2+ groups) during deposition.[72,81] Accordingly, our results (Figure 9) show a slight reduction in the apparent Mo loading at increased phosphorus concentrations in solution. This decrease c-an be explained by a lower Mo dispersion which can be attributed to a blockage of the primary sorption sites for Mo by phosphates, as a consequence of oxoanion competition.[77] The differences in surface P/Mo ratio are much lower in conditions where free phosphates are minor species in solution (AHM-based solutions or low P/Mo ratio).

The surface-dependent aggregation is directly related to the nature of the –OH sorption sites on the different α-Al_2O_3 orientations that are summarized in the introduction section (Figure 1).

It has been proposed that the R$(1\bar{1}02)$ plane has only one type of surface OH: Al_{4c}-μ_1-OH[50] that have been reported to form strong bonds with oxoanions.[24] Since phosphates are preferentially adsorbed with respect to molybdates,[72] the former will occupy first the strongest adsorption sites leading to a high dispersion of phosphates and high P/Mo ratios analyzed with XPS.

On the contrary, the surface termination of the C(0001) plane is composed of Al_{6c}-μ_2-OH sites that leads to weaker oxoanion-surface interactions[24] and consequently larger phosphate aggregation as well as larger Mo particles (low surface P/Mo ratio).

The surface structure of the A$(11\bar{2}0)$ and M$(10\bar{1}0)$ planes has been proposed to be terminated with singly, doubly and triply OH bound to 6-fold Al^{3+} (i.e. Al_{6c}-μ_1-OH, Al_{6c}-μ_2-OH, Al_{6c}-μ_3-OH) which would have intermediate oxoanion-surface interactions with respect to the two previous planes.[24] However, the results of the present work tend to show that the A$(11\bar{2}0)$ and M$(10\bar{1}0)$ planes have distinct behaviors in terms of surface P/Mo ratio and sulfidation ratio. The A$(11\bar{2}0)$ plane being close to the results for the R$(1\bar{1}02)$ plane while the M$(10\bar{1}0)$ plane is intermediate in between the R$(1\bar{1}02)$ and C(0001) planes. Such distinct behavior cannot be explained in the present knowledge of the surface structure of both surfaces. More work needs to be done on the surface structure of these two terminations at the oxide/water interface using ab-initio molecular dynamics for example.[82]

Regarding the sulfide phase, there is some agreement that phosphorus decreases the active phase-support interactions, leading to more stacked MoS_2 clusters.[39,80] In the present work, the surface-dependent sulfidation shows that the phosphorus effect is less straightforward. At high P content in solution and high surface P/Mo ratio (precursor solution from MoO_3 with P/Mo = 0.57), an important sulfidation delay and reduction in the stacking number of MoS_2 slabs is observed. While the stacking number is reduced for all crystal planes, the delay in sulfidation is especially evident for planes A$(11\bar{2}0)$ and R$(1\bar{1}02)$, which show a high phosphate dispersion and a large delay in the evolution of the sulfidation ratio with temperature. A low-temperature delay in sulfidation degree was also reported by van Haandel *et al*.[83] for Co-Mo-P and Mo-P dried, and most notably, calcined catalysts.

At this point it is important to note that a significant difference between the model catalysts used in the present work and traditional γ-Al_2O_3 porous catalysts is that the large amount of phosphates in solution is entirely available and in contact with the surface of the support for planar substrates. Phosphates can be distributed across the surface and possibly interact with all available surface –OH groups. Instead, these large quantities would not be able to reach all sorption sites on a porous material as they are preferentially adsorbed on the external surface of the extrudates.[72] The influence of phosphates can thus probably be intensified on model planar catalysts. In such a way, we can postulate that planar surfaces enhance the phosphorus effect compared to what is expected on porous support.

In the particular case of the A($11\bar{2}0$) and R($1\bar{1}02$) planes, the phosphates are well dispersed, probably as pure phosphates or $AlPO_4$ layers, in close contact with Mo oxides particles after calcination. This condition has previously been reported to favor the formation of a Mo phase strongly bonded to phosphorus and alumina sorption sites (Al-O-Mo-O-P bonds), where Mo atoms are presumably harder to reduce and sulfide to MoS_2 when they are part of this polyatomic structure.[44,78] Furthermore, a large number of small phosphate particles covering the surface would also tend to confine the Mo particle and impede their growth as MoS_2 during sulfidation. In other words, our results pinpoint a model in which large phosphate dispersion will decrease the sulfidation ratio of the Mo active phase through a large intimacy between phosphates and molybdates. Such proximity will lead to i) a chemical inhibition: molybdo-phosphate mixed structures, via the polyatomic Mo phase (Al-O-Mo-O-P bonds), are less reducible than pure molybdates, ii) a physical / diffusion inhibition: phosphates surround the Mo particle and hinder the growth of the MoS_2 particle at low temperatures. The predominant occurrence of MoS_2 single-slabs on the model catalysts prepared with the P/Mo = 0.57 solution seem to be in line with this hypothesis: phosphorus aggregates tend to impede the growth of multi-layered MoS_2 slabs through diffusion limitation of mobile Mo species. Higher sulfidation temperatures (500°C) are required to overcome surface diffusion barrier and hence to sulfide the model catalysts supported up to an extent of a similar phosphorus-free or mildly P-doped catalyst.

Conversely, for the C(0001) plane, large phosphate clusters highly disseminated on the surface will result in a reduced phosphate/molybdate intimacy leading to a lower chemical and physical inhibition of MoS_2 growth.

Figure 18 summarizes these findings for the emblematic cases of C(0001) and R($1\bar{1}02$) planes.

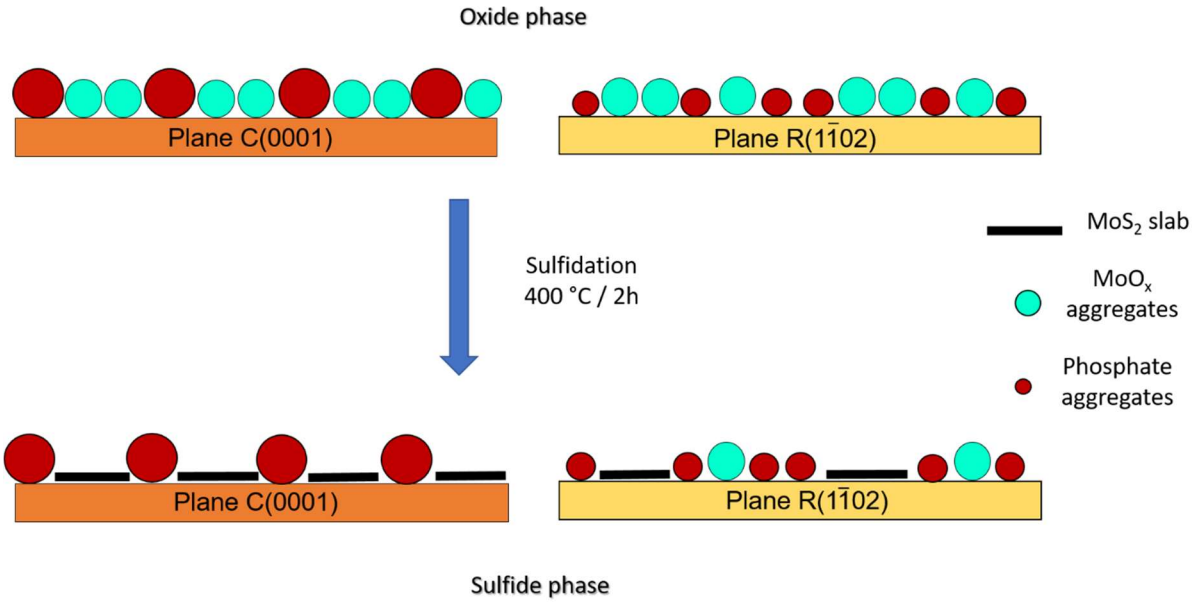

Figure 18. Schematic representation of molybdenum oxides (top), sulfides (bottom) and phosphates adsorbed on the C(0001) and R(1$\bar{1}$02) planes of α-Al_2O_3 after spin-coating of a precursor solution with initial P/Mo = 0.57, MoO_3 as Mo source, calcination and further sulfidation.

In an effort to extend the results obtained with the α-Al_2O_3 system used in this work as a surrogate for the traditional γ-Al_2O_3 support, one can consider the α-Al_2O_3 / γ-Al_2O_3 analogy proposed by Bara *et al.*[24] (see Figure 19 left). A scheme of the selectivity in phosphorus doping during spin-coating deposition and subsequent effect on the delayed sulfidation degree is presented below (Figure 19) based on the results presented in this work and suggests a surface-dependent influence of phosphorus on the predominant γ-Al_2O_3 surfaces. More specifically, considering the proposed relationship between the R(1$\bar{1}$02)/α-Al_2O_3 plane and the predominant (110)/γ-Al_2O_3 plane, our results suggest that for P-doped sulfide catalysts, the lowest sulfidation degree is achieved on the predominant (110) orientation of γ-Al_2O_3.

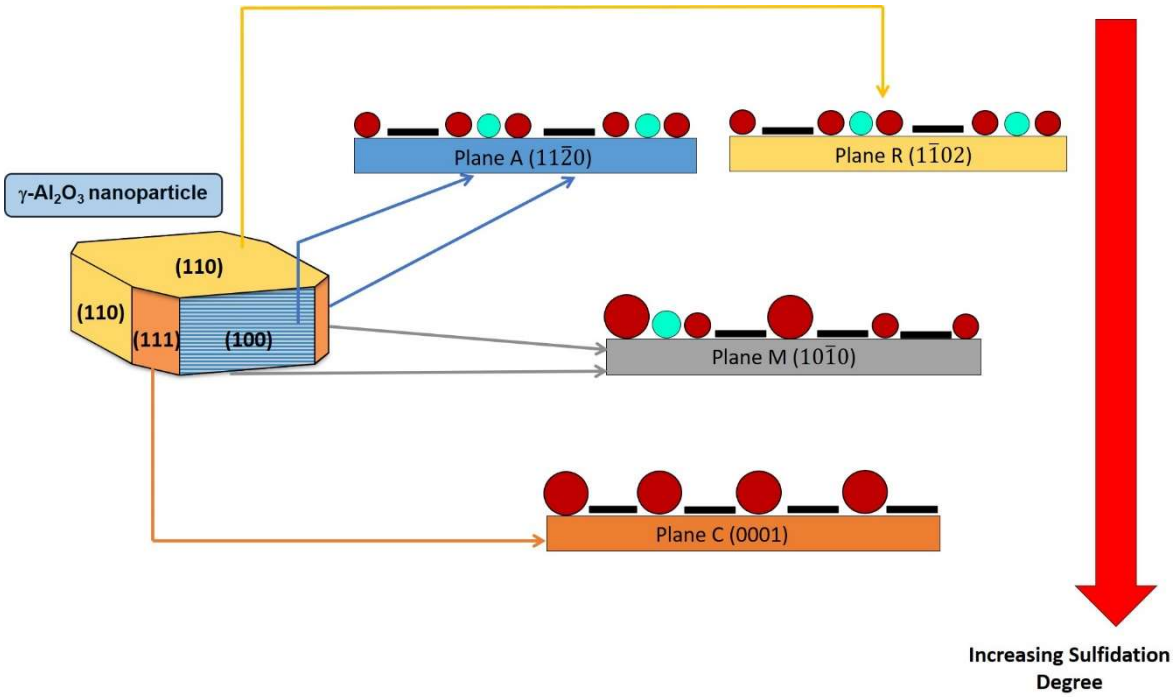

Figure 19. Scheme depicting the selectivity in the sulfidation degree for the different crystal planes of γ-Al_2O_3 in terms of a α-Al_2O_3 / γ-Al_2O_3 analogy proposed by Bara *et al.*[24,32] (same legend as Figure 18)

4. Conclusions

Model P-doped MoS_2/α-Al_2O_3 HDT catalysts were synthesized following an aqueous-phase surface-science approach in order to study the surface dependent P doping and its influence on the genesis of the active phase. Four different crystal planes of α-Al_2O_3, C(0001), A(11$\bar{2}$0), M(10$\bar{1}$0) and R(1$\bar{1}$02), were used as support for the model catalysts, as it has been postulated that their surface –OH speciation mimic the surface OH speciation of traditional γ-Al_2O_3 supports.

The planar model catalysts were prepared by spin-coating deposition of aqueous phospho-molybdic solutions since this method can mimic aqueous-phase deposition on powder supports and bring a good homogeneity of the active phase throughout the surface of the support.

Liquid-state NMR (^{31}P, ^{95}Mo) was used to precisely study the Mo and P speciation in phospho-molybdic precursor solutions for various P concentrations. This speciation is dependent both on the phosphorus content and the nature of the Mo precursor. The solutions prepared from MoO_3 and rich in phosphorus (P/Mo = 0.40 and 0.57) contained a large excess of free phosphates, as shown by liquid-state ^{31}P NMR analysis. The other phosphorus-containing species were P-Mo heteropolyanions such as $P_2Mo_5O_{23}^{6-}$ Strandberg-type HPA and lacunar Keggin $PMo_9O_{34}^{9-}$. ^{95}Mo NMR showed almost no free molybdates in the different solutions. Lower P/Mo ratio and solutions prepared from heptamolybdate showed a reduced

proportion of free phosphates. Hence, the relative proportion of phospho-molybdic HPA and free phosphates can be finely adjusted with the P content and Mo source of the impregnation solution.

XPS quantification of the surface P/Mo ratio on the model catalysts revealed a surface-dependent aggregation of phosphates after spin-coating deposition with the following decreasing aggregation order: C(0001) >> M$(10\bar{1}0)$ > A$(11\bar{2}0)$, R$(1\bar{1}02)$. The surface hydroxyls of the A$(11\bar{2}0)$ and R$(1\bar{1}02)$ planes interact more strongly with phosphates and molybdates than those of the C(0001) and M$(10\bar{1}0)$ planes, leading to an apparent higher surface P/Mo ratio, as phosphate dispersion is enhanced. Interestingly, phosphate dispersion is also enhanced for the strongly interacting surfaces when the concentration of free phosphates in the impregnation solution is high. Our results also confirm a competition between phosphates and Mo HPA for alumina sorption sites leading to small phosphate clusters covering the surface on the R$(1\bar{1}02)$ plane and large phosphate clusters more disseminated on the C(0001) plane.

The interaction between phosphate groups and the support transcends the oxide phase and impacts the sulfide active phase significantly as well. Delayed sulfidation with respect to non-doped or mildly P-doped model catalysts was observed in systems prepared with precursor solutions of high P/Mo ratio (i.e. 0.57). This effect is enhanced for model catalysts prepared on the A$(11\bar{2}0)$ and R$(1\bar{1}02)$ planes that show the highest surface P/Mo ratio (highest phosphate dispersion). Lower sulfidation is explained via two distinctive effects related to intimacy between molybdates and phosphates in highly dispersed systems: a) a chemical one through the formation of a mixed Mo-P phase in strong interaction with the alumina support (Al-O-Mo-O-P bonds) that resists sulfidation and b) a physical one, related to phosphate particles inhibiting MoS_2 growth during the genesis of the active phase. Moreover, this retardation was observed in addition to an overall reduction in the stacking number.

The surface-science approach adopted in this work with oriented α-Al_2O_3 wafers leads to an improved understanding of phosphorus-doping on real powder catalysts based on γ-Al_2O_3. The surface-dependent P dispersion and its impact on the sulfidation of the MoS_2 active phase indicate that the sulfidation degree of P-doped industrial catalysts may be heterogeneous over the different facets of γ-Al_2O_3 particles.

5. Acknowledgements

We thank Dr J. Fresnais for his help and advices on spin-coating deposition and Prof. P. Gouzerh fror fruitful discussions on the chemistry of heteropolyanions. We are also grateful to S. Casale for her support on TEM experiments, D. Montero for his support on the SEM experiments and C. Méthivier for his help in the XPS data acquisition and analysis. We thank the Institut des Matériaux de Paris Centre (IMPC FR2482) for servicing FEG-SEM & EDX instrumentation and Sorbonne Université, CNRS and C'Nano projects of the Région Ile-de-France for funding.

References

[1] European Parliament, *Off. J. Eur. Union* **2009**, L140/88-L140/113.

[2] International Maritime Organization. Resolution MEPC(58), **2008**, *176.*

[3] A. Gruia, in *Handb. Pet. Process.*, Springer Netherlands, Dordrecht, **2008**, pp. 321–354.

[4] H. Toulhoat, P. Raybaud, *Catalysis by Transition Metal Sulphides : From Molecular Theory to Industrial Application*, Editions TECHNIP, **2013**.

[5] United States Patent and Trademark Office. Patent US7737071B2, **1993.**

[6] J. Kibsgaard, J. V. Lauritsen, E. Lægsgaard, B. Clausen, H. Topsøe, F. Besenbacher, *J. Am. Chem. Soc.* **2006**.

[7] J. V. Lauritsen, S. Helveg, E. Lægsgaard, I. Stensgaard, B. S. Clausen, H. Topsøe, F. Besenbacher, *J. Catal.* **2001**, *197*, 1–5.

[8] H. Topsøe, B. S. Clausen, R. Candia, C. Wivel, S. Mørup, *J. Catal.* **1981**, *68*, 433–452.

[9] S. Helveg, J. V. Lauritsen, E. Lægsgaard, I. Stensgaard, J. K. Nørskov, B. S. Clausen, H. Topsøe, F. Besenbacher, *Phys. Rev. Lett.* **2000**, *84*, 951–954.

[10] R. Candia, O. Sørensen, Jør. Villadsen, N.-Y. Topsøe, B. S. Clausen, H. Topsøe, *Bull. des Sociétés Chim. Belges* **2010**, *93*, 763–774.

[11] C. Wivel, B. S. Clausen, R. Candia, S. Mørup, H. Topsøe, *J. Catal.* **1984**, *87*, 497–513.

[12] H. Topsøe, B. S. Clausen, *Catal. Rev.* **1984**, *26*, 395–420.

[13] B. Hinnemann, J. K. Nørskov, H. Topsøe, *J. Phys. Chem. B,* **2005**, 109, 6, 2245-2253.

[14] P. Raybaud, J. Hafner, G. Kresse, S. Kasztelan, H. Toulhoat, *J. Catal.* **2000**, *190*, 128–143.

[15] E. Krebs, B. Silvi, P. Raybaud, *Catal. Today* **2008**, *130*, 160–169.

[16] J. M. Lewis, R. A. Kydd, P. M. Boorman, P. H. Van Rhyn, *Appl. Catal. A Gen.* **1992**, *84*, 103–121.

[17] T. A. Zepeda, B. Pawelec, R. Obeso-Estrella, J. N. Díaz de León, S. Fuentes, G. Alonso-Núñez, J. L. G. Fierro, *Appl. Catal. B Environ.* **2016**, *180*, 569–579.

[18] S. Badoga, A. K. Dalai, J. Adjaye, Y. Hu, *Fuel Process. Technol.* **2017**, *159*, 232–246.

[19] V. Costa, B. Guichard, M. Digne, C. Legens, P. Lecour, K. Marchand, P. Raybaud, E. Krebs, C. Geantet, *Catal. Sci. Technol.* **2013**, *3*, 140–151.

[20] J. Escobar, A. W. Gutiérrez, M. C. Barrera, J. A. Colín, *Can. J. Chem. Eng.* **2016**, *94*, 66–74.

[21] J. Escobar, M. C. Barrera, A. W. Gutiérrez, J. E. Terrazas, *Fuel Process. Technol.* **2017**, *156*, 33–42.

[22] R. Thomas, E. M. van Oers, V. H. J. de Beer, J. Medema, J. A. Moulijn, *J. Catal.* **1982**, *76*, 241–253.

[23] M. Digne, P. Sautet, P. Raybaud, P. Euzen, H. Toulhoat, *J. Catal.* **2004**, *226*, 54–68.

[24] C. Bara, A. F. Lamic-Humblot, E. Fonda, A. S. Gay, A. L. Taleb, E. Devers, M. Digne, G. D. Pirngruber, X. Carrier, *J. Catal.* **2016**, *344*, 591–605.

[25] C. Bara, L. Plais, K. Larmier, E. Devers, M. Digne, A.-F. Lamic-Humblot, G. D. Pirngruber, X. Carrier, *J. Am. Chem. Soc.* **2015**, *137*, 15915–15928.

[26] Y. Sakashita, T. Yoneda, *J. Catal.* **1999**, *185*, 487–495.

[27] H. Shimada, *Catal. Today* **2003**, *86*, 17–29.

[28] C. Zhang, M. Brorson, P. Li, X. Liu, T. Liu, Z. Jiang, C. Li, *Appl. Catal. A Gen.* **2019**, *570*, 84–95.

[29] A. Centeno, E. Laurent, B. Delmon, *J. Catal.* **1995**, *154*, 288–298.

[30] Y. Araki, K. Honna, H. Shimada, *J. Catal.* **2002**, *207*, 361–370.

[31] J. Lee, E. J. Jang, H. Y. Jeong, J. H. Kwak, *Appl. Catal. A Gen.* **2018**, *556*, 121–128.

[32] C. Bara, E. Devers, M. Digne, A.-F. Lamic-Humblot, G. D. Pirngruber, X. Carrier, *ChemCatChem* **2015**, *7*, 3422–3440.

[33] Y. Sakashita, *Surf. Sci.* **2001**, *489*, 45–58.

[34] R. Prins, V. H. J. De Beer, G. A. Somorjai, *Catal. Rev.* **1989**, *31*, 1–41.

[35] G. Kresse, M. Schmid, E. Napetschnig, … M. S.-, undefined 2005, *science.sciencemag.org* **n.d.**

[36] O. V. Klimov, K. A. Nadeina, Y. V. Vatutina, E. A. Stolyarova, I. G. Danilova, E. Y. Gerasimov, I. P. Prosvirin, A. S. Noskov, *Catal. Today* **2018**, *307*, 73–83.

[37] Y. V. Vatutina, O. V. Klimov, E. A. Stolyarova, K. A. Nadeina, I. G. Danilova, Y. A. Chesalov, E. Y. Gerasimov, I. P. Prosvirin, A. S. Noskov, *Catal. Today* **2019**, *329*, 13–23.

[38] K. A. Nadeina, M. O. Kazakov, I. G. Danilova, A. A. Kovalskaya, E. A. Stolyarova, P. P. Dik, E. Y. Gerasimov, I. P. Prosvirin, Y. A. Chesalov, O. V. Klimov, et al., *Catal. Today* **2019**, *329*, 2–12.

[39] R. Iwamoto, J. Grimblot. *Advances in Catalysis, V. 44*, Influence of Phosphorus on the Properties of Alumina-Based Hydrotreating Catalysts, pp. 417-502 (2000).

[40] A. Griboval, P. Blanchard, E. Payen, M. Fournier, J. L. Dubois, *Catal. Today* **1998**, *45*, 277–283.

[41] A. Griboval, P. Blanchard, E. Payen, M. Fournier, J. . Dubois, J. . Bernard, *Appl. Catal. A Gen.* **2001**, *217*, 173–183.

[42] A. Griboval, P. Blanchard, L. Gengembre, E. Payen, M. Fournier, J. L. Dubois, J. R. Bernard, *J. Catal.* **1999**, *188*, 102–110.

[43] M. Jian, R. Prins, *Bull. des Sociétés Chim. Belges* **2010**, *104*, 231–236.

[44] J. L. G. Fierro, A. Lo´pez Agudo*, N. Esquivel, R. Lo´pez Cordero, *Appl. Catal.* **1989**, *48*, 353–363.

[45] R. M. van Hardeveld, P. L. J. Gunter, L. J. van IJzendoorn, W. Wieldraaijer, E. W. Kuipers, J. W. Niemantsverdriet, *Appl. Surf. Sci.* **1995**, *84*, 339–346.

[46] G. Prieto, F. Schüth, *J. Catal.* **2015**, *328*, 59–71.

[47] D. B. Hall, P. Underhill, J. M. Torkelson, *Polym. Eng. Sci.* **1998**, *38*, 2039–2045.

[48] M. Digne, P. Sautet, P. Raybaud, P. Euzen, H. Toulhoat, *J. Catal.* **2004**, *226*, 54–68.

[49] A. Marmier, S. C. Parker, *Phys. Rev. B* **2004**, *69*, 115409.

[50] A. Tougerti, C. Méthivier, S. Cristol, F. Tielens, M. Che, X. Carrier, *Phys. Chem. Chem. Phys.* **2011**, *13*, 6531.

[51] V. Costa, Compréhension Du Rôle Des Additifs Du Type Glycol Sur l'amélioration Des Performances Des Catalyseurs d'hydrotraitement, Doctoral Dissertation, IFPEN-Université Lyon 1, **2008**.

[52] A. D. Gandubert, C. Legens, D. Guillaume, E. Payen, *Surf. Interface Anal.* **2006**, *38*, 206–209.

[53] A. D. Gandubert, C. Legens, D. Guillaume, S. Rebours, E. Payen, *Oil Gas Sci. Technol. - Rev. l'IFP* **2007**, *62*, 79–89.

[54] Casa software Ltd, **2009**, 342.

[55] S. N. Towle, G. E. Brown, G. A. Parks, *J. Colloid Interface Sci.* **1999**, *217*, 299–311.

[56] S. Tanuma, C. J. Powell, D. R. Penn, *Surf. Interface Anal.* **1994**, *21*, 165–176.

[57] C. A. Schneider, W. S. Rasband, K. W. Eliceiri, *Nat. Methods* **2012**, *9*, 671–5.

[58] L. Pettersson, I. Andersson, L. O. Oehman, *Inorg. Chem.* **1986**, *25*, 4726–4733.

[59] J. A. Bergwerff, Spatially Resolved Spectroscopy on the Preparation of CoMo/Al2O3 Hydrodesulphurization Catalysts, Doctoral Dissertation, Utrecht University, **2007**.

[60] J. A. R. van Veen, O. Sudmeijer, C. A. Emeis, H. de Wit, *J. Chem. Soc. Dalt. Trans.* **1986**, *0*, 1825.

[61] A. Griboval, P. Blanchard, E. Payen, M. Fournier, J. L. Dubois, *Catal. Today* **1998**, *45*, 277–283.

[62] L. Pettersson, I. Andersson, L.O. Öhman, *Acta Chem. Scand.* **1985**, *39a*, 53-58.

[63] H. Kraus, R. Prins, *J. Catal.* **1997**, *170*, 20–28.

[64] J. A. R. Van Veen, P. A. J. M. Hendriks, R. R. Andrea, E. J. G. M. Romers, A. E. Wilson, *J. Phys. Chem.* **1990**, *94*, 5282–5285.

[65] G. Hervé, A. Tézé, R. Contant, in *Polyoxometalate Mol. Sci.*, Springer Netherlands, Dordrecht, **2003**, pp. 33–54.

[66] J. A. R. Van Veen, O. Sudmeijer, C. A. Emeis, H. De Wit, *J. Chem. Soc. Dalt. Trans.* **1986**, 1825–1831.

[67] M. A. Fedotov, R. I. Maksimovskaya, *J. Struct. Chem.* **2006**, *47*, 952–978.

[68] R. I. Maksimovskaya, G. M. Maksimov, *Inorg. Chem.* **2007**, 46, 9, 3688-3695.

[69] L. P. Kazansky, T. Yamase, *J. Phys. Chem. A* **2004**, 108, 30, 6437-6448.

[70] M. A. Fedotov, *Bull. Acad. Sci. USSR Div. Chem. Sci.* **1984**, *33*, 1070–1072.

[71] H. Kraus, R. Prins, *J. Catal.* **1996**, *164*, 251–259.

[72] J. A. Bergwerff, L. G. A. van de Water, T. Visser, P. de Peinder, B. R. G. Leliveld, K. P. de Jong, B. M. Weckhuysen, *Chem. - A Eur. J.* **2005**, *11*, 4591–4601.

[73] T. K. T. Ninh, L. Massin, D. Laurenti, M. Vrinat, *Appl. Catal. A Gen.* **2011**, *407*, 29–39.

[74] D. Laurenti, B. Phung-Ngoc, C. Roukoss, E. Devers, K. Marchand, L. Massin, L. Lemaitre, C. Legens, A.-A. Quoineaud, M. Vrinat, *J. Catal.* **2013**, *297*, 165–175.

[75] R. Cattaneo, T. Weber, T. Shido, R. Prins, *J. Catal.* **2000**, *191*, 225–236.

[76] M. Sun, D. Nicosia, R. Prins, *Catal. Today* **2003**, *86*, 173–189.

[77] S. Il Kim, S. Ihl Woo, *J. Catal.* **1992**, *133*, 124–135.

[78] O. Poulet, R. Hubaut, S. Kasztelan, J. Grimblot, *Bull. des Sociétés Chim. Belges* **2010**, *100*, 857–863.

[79] L. P. Hansen, E. Johnson, M. Brorson, S. Helveg, *J. Phys. Chem. C* **2014**, *118*, 22768–22773.

[80] F. Rashidi, T. Sasaki, A. M. Rashidi, A. Nemati Kharat, K. J. Jozani, *J. Catal.* **2013**, *299*, 321–335.

[81] J. A. R. Van Veen, P. A. J. M. Hendriks, R. R. Andrea, E. J. G. M. Romers, A. E. Wilson, *J. Phys. Chem.* **1990**, *94*, 5282–5285.

[82] B. F. Ngouana-Wakou, P. Cornette, M. Corral Valero, D. Costa, P. Raybaud, *J. Phys. Chem. C* **2017**, *121*, 10351–10363.

[83] L. van Haandel, G. M. Bremmer, E. J. M. Hensen, T. Weber, *J. Catal.* **2017**, *351*, 95–106.